SANDIA REPORT

SAND2005-0951
Unlimited Release
Printed March 2005

Parametric Studies of Penetration Events: A Design and Analysis of Experiments Approach

E. B. Marin, M. L. Chiesa, P. M. Booker

Prepared by
Sandia National Laboratories
Albuquerque, New Mexico 87185 and Livermore, California 94550

Sandia is a multiprogram laboratory operated by Sandia Corporation, a Lockheed Martin Company, for the United States Department of Energy's National Nuclear Security Administration under Contract DE-AC04-94AL85000.

Approved for public release; further dissemination unlimited.

Sandia National Laboratories

Issued by Sandia National Laboratories, operated for the United States Department of Energy by Sandia Corporation.

Available to DOE and DOE contractors from
U.S. Department of Energy
Office of Scientific and Technical Information
P.O. Box 62
Oak Ridge, TN 37831

Telephone: (865)576-8401
Facsimile: (865)576-5728
E-Mail: reports@adonis.osti.gov
Online ordering: http://www.osti.gov/bridge

Available to the public from
U.S. Department of Commerce
National Technical Information Service
5285 Port Royal Rd
Springfield, VA 22161

Telephone: (800)553-6847
Facsimile: (703)605-6900
E-Mail: orders@ntis.fedworld.gov
Online order: http://www.ntis.gov/help/ordermethods.asp?loc=7-4-0#online

SAND2005-0951
Unlimited Release
Printed February 2005

Parametric Studies of Penetration Events: A Design and Analysis of Experiments Approach

Esteban B. Marin
Science-Based Materials Modeling

Michael L. Chiesa
Engineering Mechanics Modeling & Simulation

Paul M. Booker
W84 & Advanced Systems

Sandia National Laboratories
P.O.Box 969
Livermore, CA 94551

Abstract

A numerical screening study of the interaction between a penetrator and a geological target with a preformed hole has been carried out to identify the main parameters affecting the penetration event. The planning of the numerical experiment was based on the orthogonal array OA(18,7,3,2), which allows 18 simulation runs with 7 parameters at 3 levels each. The strength of 2 of the array allows also for two-factor interaction studies. The seven parameters chosen for this study are: penetrator offset, hole diameter, hole taper, vertical and horizontal velocity of the penetrator, angle of attack of the penetrator and target material. The analysis of the simulation results has been based on main effects plots and analysis of variance (ANOVA), and it has been performed using three metrics: the maximum values of the penetration depth, penetrator deceleration and plastic strain in the penetrator case. This screening study shows that target material has a major influence on penetration depth and penetrator deceleration, while penetrator offset has the strongest effect on the maximum plastic strain.

Keywords: penetration modeling, parametric study, design of experiments, analysis of variance

Acknowledgments

Sandia is a multi-program laboratory operated by Sandia Corporation, a Lockheed Martin Company, for the United States Department of Energy's National Nuclear Security Administration under contract DE-AC04-94AL85000. The first author thanks Arlo F. Fossum and Monica L. Martinez-Canales for the productive discussions regarding the Fossum's geological model and the design of experiments approach, respectively.

Contents

List of Figures

List of Tables

1. Introduction

Earth penetration capabilities are critical to maintain a credible deterrent for the future. To enhance the flexibility of these capabilitites, lightweight earth penetrator weapons (1000lb class) that have the potential to utilize various delivery platforms are currently under study. These lightweight penetrators generally experience larger deceleration loads and less depth of penetration compared with large earth penetrators, and hence, methods to improve their penetrability and survivability by preconditioning the target with a precursor shaped charge hole are employed, see Figure 1.1. The benefits of enhancing earth penetration of lightweight "follow through" penetrators with a precursor shaped charge has been documented since the late 1960s, in the context of the DUCAT project (Patterson and Fellerhoff, 1971) and other programs at Sandia National Laboratories. More recent work continues to explore enhanced penetration with shape charges (Baty, *et al.*, 2003; Vigil, 2003).

Modeling and simulation play an important role in the analysis and prediction of penetration events, in particular when specific design concepts are explored, such as the shaped charge follow through penetrator concept. Generally, in this design, the shaped charge and penetrator fit in the existing volume of the delivery system (cruise missile), with the shape charge preceding the penetrator. When the shape charge is detonated above the target, the resulting jet penetrates the target, producing a "pilot" hole with a defined profile that aids the penetration process by both producing deeper penetration depths and reducing the penetrator deceleration loads. Typically, the penetration is considered successful if the penetrator sticks in the target and survives with minimal structural damage so that the weapon components inside the penetrator function properly at maximum penetration depth. These functionality requirements impose severe restrictions on the penetration depth, penetrator deceleration loads (g-loads) and structural integrity of the penetrator case.

As in any real physical system, a penetration event displays random variations from a variety of sources, including the geometry of the problem and boundary/initial conditions. Specifically, uncertainties of the parameters defining the penetrator–target system (see Figure 1.1) may arise from variations of the external loads imposed on the penetrator (due to offset and reverse blast from shape charge detonation), variations of the hole geometry formed by the shaped charge jet, and variations about the specific geological medium to be

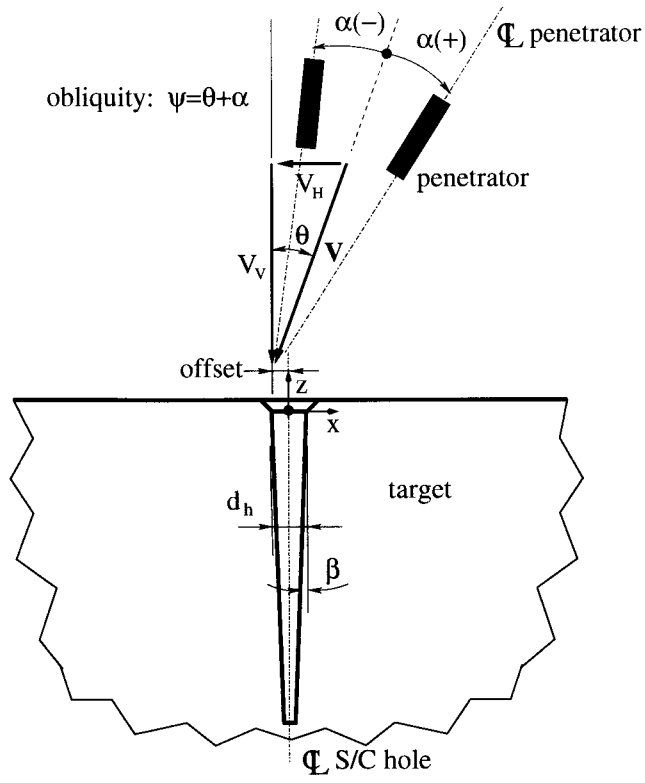

Figure 1.1: Schematic of follow through penetrator and shaped charge pilot hole concept: definition of factors (parameters) for screening study of penetration event.

penetrated, not to mention the variations in the model parameters used for the constitutive models for the target and penetrator materials. This inherently nondeterministic nature of the problem calls for a characterization of the uncertainty present as a necessary step in modeling the penetration event. Mathematically, such characterization can be accomplished by specifying probability distribution functions for the parameters defining the penetration process. Of course, the assumed uncertainty in the parameters manifest itself as uncertainty in the output of the penetration event.

The design and analysis of computer experiments (DACE) is a widely used tool for modeling and simulation of complex engineering systems, such as penetration events. A particular aspect of this approach is that it provides a systematic procedure to characterize the response of a system to variations of the system parameters. Such procedure relies on the design of the simulation runs using a sampling methodology of the parameter space, and the analysis of the simulation results using statistical and/or probabilistic techniques to identify both trends on the system response and the parameters that mostly contribute to the

response variation. This system characterization is useful for model verification, calibration and optimization.

The sampling-based methodology using a DACE approach is illustrated in Figure 1.2. Basic steps of the approach are (i) the design or planning of the experiment, which includes selecting the parameters that are involved in the analysis, their range of variation, their probability distribution functions, and the corresponding design matrix specifying the cases to be run; (ii) the evaluation of the model by numerical simulation of each case to generate the output distribution of the responses of interest (performance metrics), and (iii) the analysis of the numerical results to quantify the variation in the model response (uncertainty quantification) and/or to determine the effects or relative contribution of each parameter to the response variability (screening and sensitivity studies).

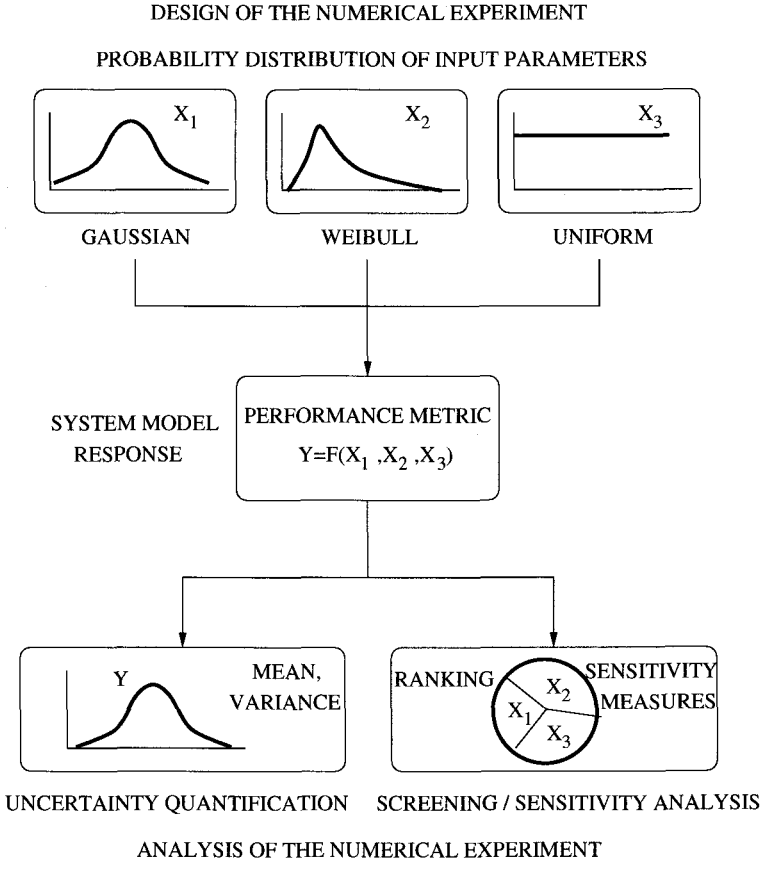

Figure 1.2: The DACE approach for engineering system analysis.

In this document, we carry out a numerical screening study of the follow through penetrator–preconditioned target system using a DACE methodology to identify the main parameters or factors affecting the penetration event. The system configuration used in this study is

presented in Figure 1.1. Note that for simplicity we assume that the centerline of the pilot hole is vertically aligned, although in practice is it typically formed at a certain angle with the vertical, depending on the obliquity of the cruise missile type delivery system. Also, given the preliminary nature of this study, it is assumed that the factors have a uniform probability distribution in their selected range of variation or levels. As such, we consider a three-level factor numerical experiment in order to detect curvature effects in the response. Note that, since the probabilistic interpretation of the inputs carries over to the system response, the performance measures or metrics will also have a uniform distribution. This screening study is planned using an orthogonal array and the trends in the system response for the ranking of the selected parameters is extracted using graphical and statistical tools (main/interaction effects plots and analysis of variance). The chosen metrics for this study are the maximum values of the penetration depth (u_{zMAX}), penetrator deceleration (a_{zMAX}) and plastic strain in the penetrator case (ϵ^p_{MAX}). It is important to note that plastic strain is used here as an indicator of the severity of the penetrator case deformation, and not as a failure parameter (for which ϵ^p may not be an adequate variable).

For presentation purposes, the document is organized as follows. Section 2 describes the DACE planning of the numerical experiment using orthogonal arrays. Section 3 shows the results of the numerical simulations carried out using an orthogonal-array-based design matrix. Section 4 presents the DACE analysis of these results using graphical and statistical tools. In this section, main effects and two factor interaction are studied. Section 5 extends the discussion of the DACE numerical results by comparing them with the results obtained from one-factor-at-a-time (OAT) numerical experiments. Finally, section 6 presents some concluding remarks.

2. Planning of the Numerical Experiment

Designing a priori a numerical experiment is an important step in the DACE approach. The design mainly consists of selecting the combination of factor levels that will provide the most information on the input-output relationship of a model in the presence of variation. Among the many designs that have been proposed for using with a DACE approach (Giunta, *et al.*, 2003), in this work we use orthogonal arrays since they allow for accomodating the discrete nature (uniform distribution) of the factor levels selected for the penetration study.

Table 2.1: Factors and levels for parametric studies.

Factor	Level 0	Level 1	Level 2
A. Offset (in)	0.0	-1.5	-3.0
B. Vertical Velocity V_V (ft/sec)	-800.0	-1000.0	-1200.0
C. Horizontal Velocity V_H (ft/sec)	0.0	-15.0	-30.0
D. Angle of attack α (degrees)	-2.0	0.0	2.0
E. Target material	CSPC	Limestone	Antelope Tuff
F. Hole diameter d_h (in)	7.5	10.0	13.0
G. Hole taper β (degrees)	0.0	0.5	1.0

Seven factors are chosen for the screening study of the penetration event. These factors, displayed in Figure 1.1, are: penetrator offset, hole diameter (d_h), hole taper (β), vertical (V_V) and horizontal (V_H) velocity of the penetrator, angle of attack (α) of the penetrator and target material. The corresponding factor levels are presented in Table 2.1, where each of the three levels are indicated with the numbers 0, 1 and 2, respectively. Based on current technologies (e.g. Vigil, 2003), the selected values are considered an adequate sampling of the parameter space. Note that the target material is taken as a qualitative factor in the analysis.

Given the number of factors and levels, we choose for the design of the numerical experi-

Table 2.2: Orthogonal Array used for screening study.

OA(18,7,3,2)						
0	0	0	0	0	0	0
1	1	1	1	1	1	0
2	2	2	2	2	2	0
0	0	1	2	1	2	0
1	1	2	0	2	0	0
2	2	0	1	0	1	0
0	1	0	2	2	1	1
1	2	1	0	0	2	1
2	0	2	1	1	0	1
0	2	2	0	1	1	1
1	0	0	1	2	2	1
2	1	1	2	0	0	1
0	1	2	1	0	2	2
1	2	0	2	1	0	2
2	0	1	0	2	1	2
0	2	1	1	2	0	2
1	0	2	2	0	1	2
2	1	0	0	1	2	2

ment the orthogonal array OA(18,7,3,2)* (Hedayat *et al.*, 1999), which is shown in Table 2.2. This design allows for 18 simulation runs with 7 parameters at 3 levels each. The strength of 2 of this array allows also for a two-factor interaction analysis. The detailed design matrix for the computer experiments constructed using this orthogonal array and Table 2.2 is presented in Table 2.3. This table gives the combination of factor levels (treatments) to be used for the simulation runs. It also shows the computed angle of obliquity of the penetrator.

The penetrator geometry is a modified BLU-109, and consists of a 3.0 CRH ogival nose with a total length of $l_p = 64$ in, and an aft-body diameter of $d_p = 14.5$ in. The total weight of the penetrator is 1048 lbs. The target geometry considered is a circular cylinder with a diameter of $D_T = 400$ in and a height of $H_T = 300$ in. The corresponding three-dimensional finite element meshes used for the penetrator and target are presented in Figure 3. Due to symmetry about the x-z plane (see Figure 1.1), only half of the penetrator-target system is modeled. The penetrator mesh includes some detail of the internal components, and consists of 212,811 8-node brick elements. The case and nose, assumed to be joined by welding, are

*The standard notation for orthogonal arrays is OA(N, k, s, t), with $N = \lambda s^t$. This notation reads as "an N–orthogonal array of strength t and index λ with k factors each at s levels". The orthogonality property means that for any t columns of the $N \times k$ matrix ($t < k$), each ordered t–tuple appears exactly λ times. There are only certain values of the integers N, k, s, t, λ that give a matrix that satisfies orthogonality, i.e., orthogonal array generation is not a trivial process.

Table 2.3: Detailed design matrix and angle of obliquity of penetrator.

Run	Factor A	B	C	D	E	F	G	Obliquity Ψ (degrees)
1	0.0	-800.0	0.0	-2.0	CSPC	7.5	0.0	-2.000
2	-1.5	-1000.0	-15.0	0.0	Limestone	10.0	0.0	0.859
3	-3.0	-1200.0	-30.0	2.0	Tuff	13.0	0.0	3.432
4	0.0	-800.0	-15.0	2.0	Limestone	13.0	0.0	3.074
5	-1.5	-1000.0	-30.0	-2.0	Tuff	7.5	0.0	-0.282
6	-3.0	-1200.0	0.0	0.0	CSPC	10.0	0.0	0.000
7	0.0	-1000.0	0.0	2.0	Tuff	10.0	0.5	2.000
8	-1.5	-1200.0	-15.0	-2.0	CSPC	13.0	0.5	-1.284
9	-3.0	-800.0	-30.0	0.0	Limestone	7.5	0.5	2.147
10	0.0	-1200.0	-30.0	-2.0	Limestone	10.0	0.5	-0.568
11	-1.5	-800.0	0.0	0.0	Tuff	13.0	0.5	0.000
12	-3.0	-1000.0	-15.0	2.0	CSPC	7.5	0.5	2.859
13	0.0	-1000.0	-30.0	0.0	CSPC	13.0	1.0	1.718
14	-1.5	-1200.0	0.0	2.0	Limestone	7.5	1.0	2.000
15	-3.0	-800.0	-15.0	-2.0	Tuff	10.0	1.0	-0.926
16	0.0	-1200.0	-15.0	0.0	Tuff	7.5	1.0	0.716
17	-1.5	-800.0	-30.0	2.0	CSPC	10.0	1.0	4.147
18	-3.0	-1000.0	0.0	-2.0	Limestone	13.0	1.0	-2.000

modeled with the BCJ elasto-viscoplastic-damage model (Bammann, 1990), while the internal components were represented with a standard linear hardening elasto-plastic model. The material parameters for the BCJ model are for AISI 4340 steel. On the other hand, nine finite element meshes were constructed for the target to accomodate the different combinations of hole diameter and hole taper given in Table 2.1. The number of finite elements for the target then varied from 745,550 ($d_h = 7.5$ in, $\beta = 1.0^o$) to 790,804 ($d_h = 10$ in, $\beta = 0.0^o$) 8-node brick elements. The response of the target material is modeled using Fossum's geological model (Fossum and Fredrich, 2000), with material properties corresponding to Conventional Strength Portland Concrete (CSPC), Limestone and Antelope Tuff. We point out here that the penetration resistance of geological materials is typically characterized by their bulk modulus (K) and porosity (φ). As such, Antelope Tuff ($K = 1128$ ksi, $\varphi = 0.380$) will offer less resistance to penetration than Limestone ($K = 1885$ ksi, $\varphi = 0.084$) and CSPC ($K = 2284$ ksi, $\varphi = 0.093$) due to its lower bulk modulus and higher porosity. Also, the penetrator-target sliding interface is modeled using a Coulomb friction law with a constant friction coefficient of $\mu = 0.04$ (Chen, 1989). In addition, given the high ratio $D_T/d_p \approx 27$, the target will effectively behave as an infinite medium in the simulations, and hence the non-reflecting boundary conditions on the outer surface of the target are not used here. A sample of the penetrator-target assembly for the simulation runs is also shown in Figure 2.1.

The 18 simulations are performed with PRESTO, an explicit dynamic Lagrangian finite element code that forms part of the Sierra framework. All the cases are run in parallel using 32 computing nodes (64 processors) on Sandia's Institutional Computing Cluster. Each node is a dual 3.06 GHz Xeon processor with 2 GB of RAM running RedHat Linux 7.3. The prescribed time interval for the penetration event is 0.012 sec, and a typical run takes on the order of 100,000 time steps (around 30 hours of CPU time).

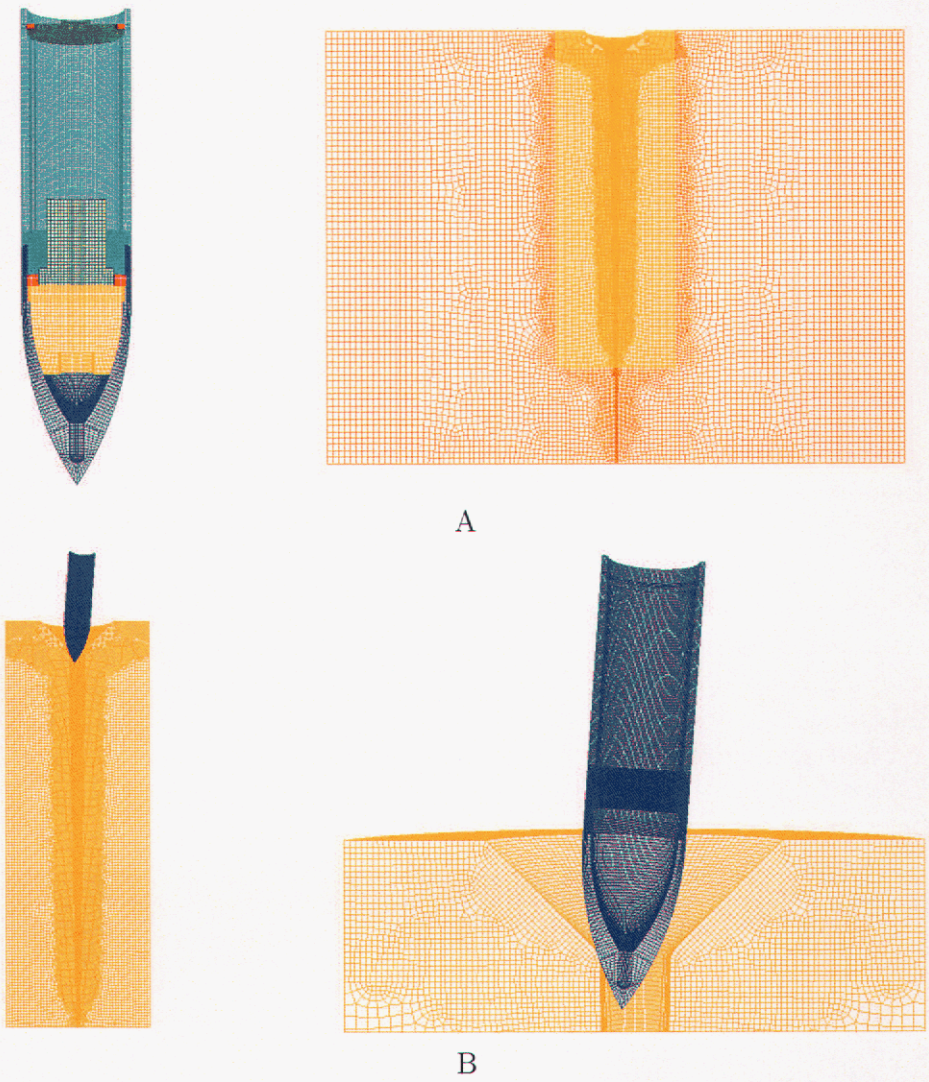

Figure 2.1: Three-dimensional finite element meshes used for penetration study. (A) Follow through penetrator and a typical preconditioned target. (B) Assembly of penetrator and target (inner core) for run 17.

3. Simulation Results

This section presents the numerical results obtained from the 18 simulation runs specified by the design matrix given in Table 2.3. The presentation is focussed on describing some qualitative features of the penetration event as related to the effect of some parameters on the response metrics. The computed normalized metrics u_{zMAX}/d_p, a_{zMAX}/g and ϵ^p_{MAX} (g is the gravity acceleration) are then given and used in the next section to study each factor's effect.

The penetration event for run 18 (see Table 2.3) and the corresponding history of penetration depth (displacement u_z) are shown in Figure 3.1. The displacement u_z is computed at a point located in the middle of the penetrator case. In this simulation, one can observe that the penetrator sticks in the target but it does not survive. The maximum normalized penetration depth is $|u_z|_{MAX}/d_p \approx 3.4$, while the maximum normalized vertical deceleration is on the order of $a_z/g \approx 9778$, see Table 3.1. This high deceleration will produce critical g-loads on the internal components of the penetrator, which may then not function properly. For this run, the penetrator case should fracture very early in the process at locations close to the joint between the case and the nose due to the high bending loads (plastic strains on the order of $\epsilon^p_{MAX} \approx 9$) imposed by the target during the penetration process.

Run 18 seems to be the worst case scenario with respect to the structural integrity of the penetrator due to the high plastic strains induced in the penetrator case. These unrealistic strain values computed from the BCJ model are obtained because the finite elements in the joint area lose about 99% of their load carrying capacity early in the process, as indicated by Figure 3.2. This Figure shows the evolution with time of vonMises stress ($\bar{\sigma}$), damage* (ϕ) and plastic strain (ϵ^p) for two elements (68308 and 44627) located in the joint area. In these elements, the stress state induces a sharp increase in damage (growth of voids) at times $0.001s$ and $0.0035s$, respectively, to a value of 0.99, leading to a rapid decrease of the stress carrying capacity of the elements, and hence to an uncontrolled accumulation of plastic strain. A better approach to model this aspect of the penetration event would be to use the kill element option in PRESTO once damage reaches a critical value, say $\phi = 0.15$.

*Damage is an internal state variable used by the BCJ model to represent the evolution of voids or porosity in structural materials, a precursor to the creation of cracks in the material

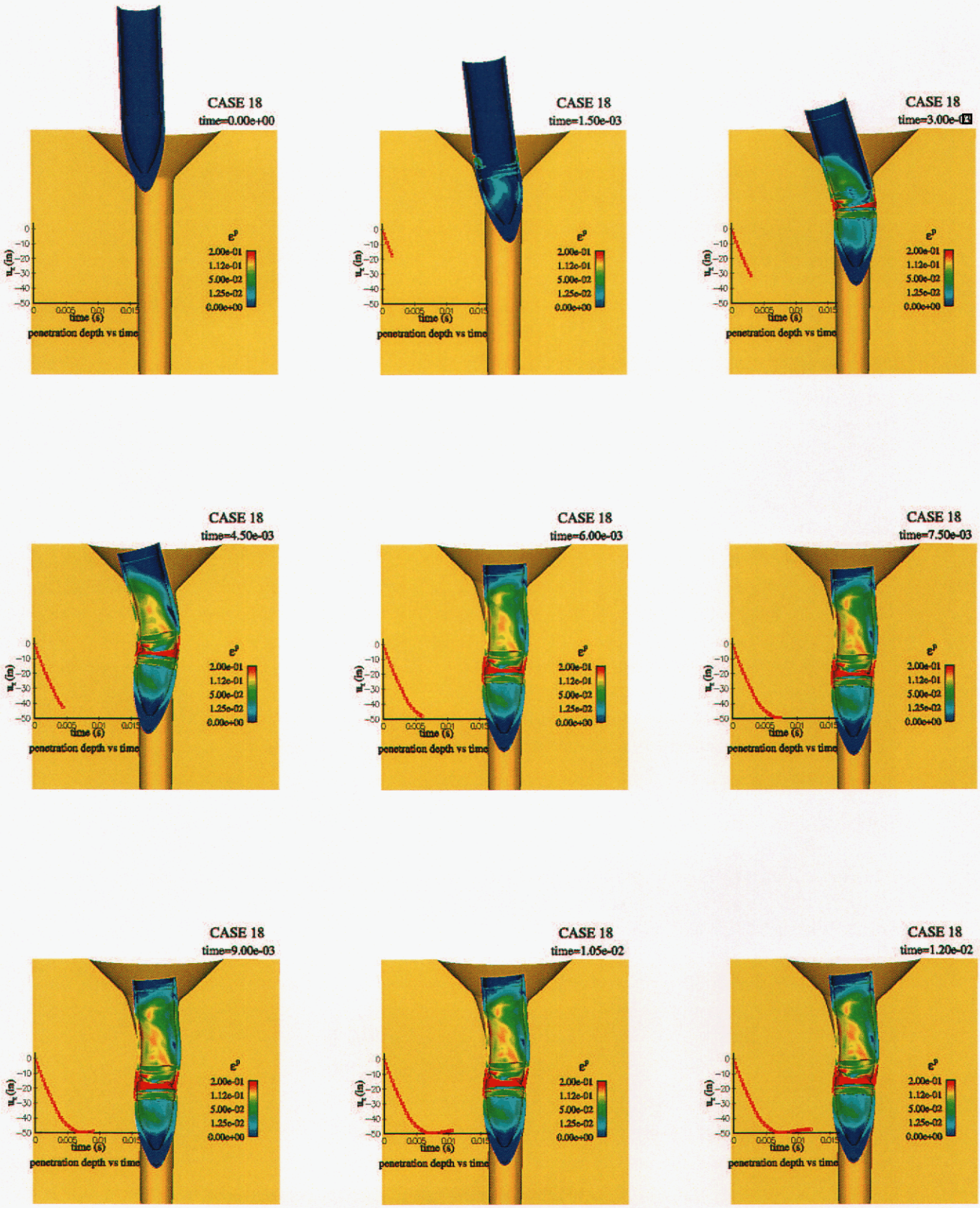

Figure 3.1: Penetration event - Run (Case) 18.

This approach avoids such high unrealistic strain, and will be used in a subsequent study. For this work, we will continue using the computed plastic strains as an indicative metric of the severity of the penetrator deformation.

The final position of the penetrator for the 18 simulation runs is presented in Figures 3.3–3.5. These figures also show the history of penetration depth and vertical acceleration at a point located at the middle of the penetrator case, as well as the history of maximum plastic strain in the penetrator case. As seen from these figures, the outcome of the penetration event can be diverse, depending on the specific factor levels used in the simulations. Here, one has to keep in mind that, for each simulation, all the factors are varied at the same time, and hence typical interpretations of the results as it is done when one-factor-at-a-time (OAT) analysis (Campolongo and Saltelli, 2000) is used may not be generally valid. The OAT approach ignores the simultaneous variation of other parameter values, an effect that may be important when the global response of the system (main effects and interactions) is nonlinear. Therefore, for a strict and robust interpretation of the DACE simulation results, one has to resort to statistical techniques such as analysis of variance.

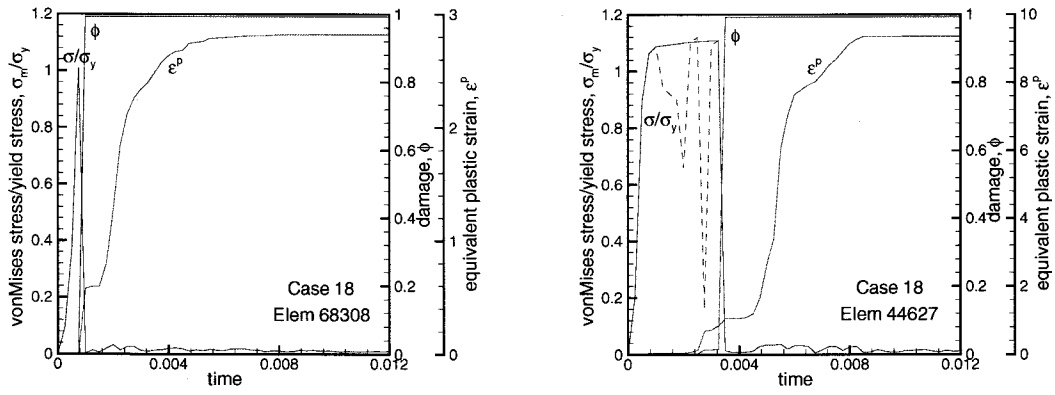

Figure 3.2: History of σ_m/σ_y (σ_y is the yield stress), ϕ and ϵ^p for two elements in the case-nose joint area. The discontinuous lines shown in the stress history for element 44627 are due to reflective stress waves in the penetrator case. The solid line indicates the stress response without such effect.

In general, however, one can make some qualitative remarks from Figures 3.3–3.5 regarding the outcome of the penetration event and its relation to specific factors. Consider, for example, the penetration depth and maximum decelerations. One can observe from these figures that, for runs 3,5,7,11,15 and 16, where the target material is Antelope Tuff, the penetrator sticks in the target and survives the penetration event. These cases give deeper penetration depths (average $|u_z|_{MAX}/d_p \approx 6.8$) and lower maximum deceleration (average $a_{zMAX}/g \approx 2883$) than the ones obtained using CSPC and Limestone as target materials (average penetration depth $|u_z|_{MAX}/d_p \approx 2.5$ and average deceleration $a_{zMAX}/g \approx 8760$).

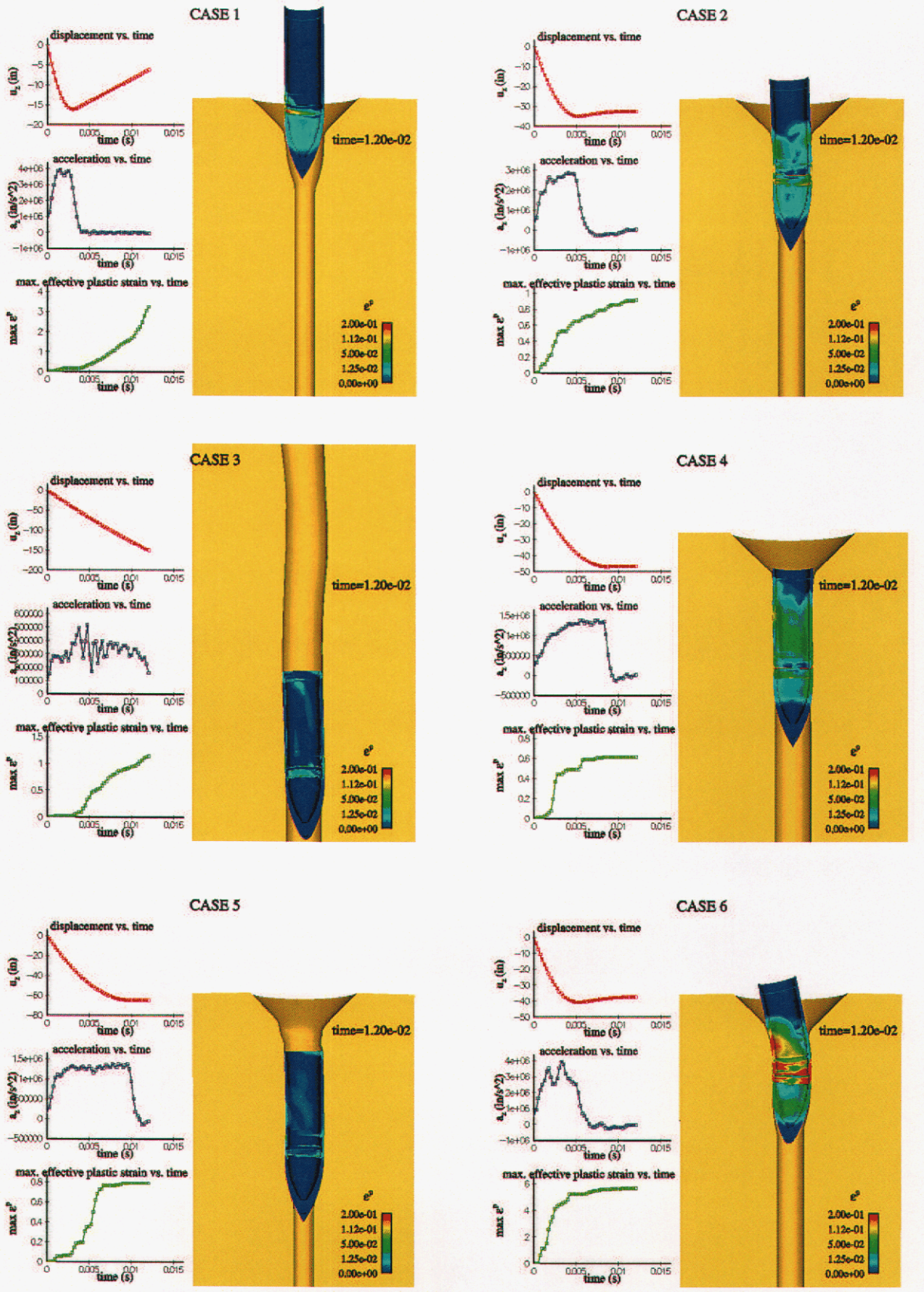

Figure 3.3: Final position of follow through penetrator and time history of displacement, acceleration and maximum effective plastic strain during penetration event, cases 1-6.

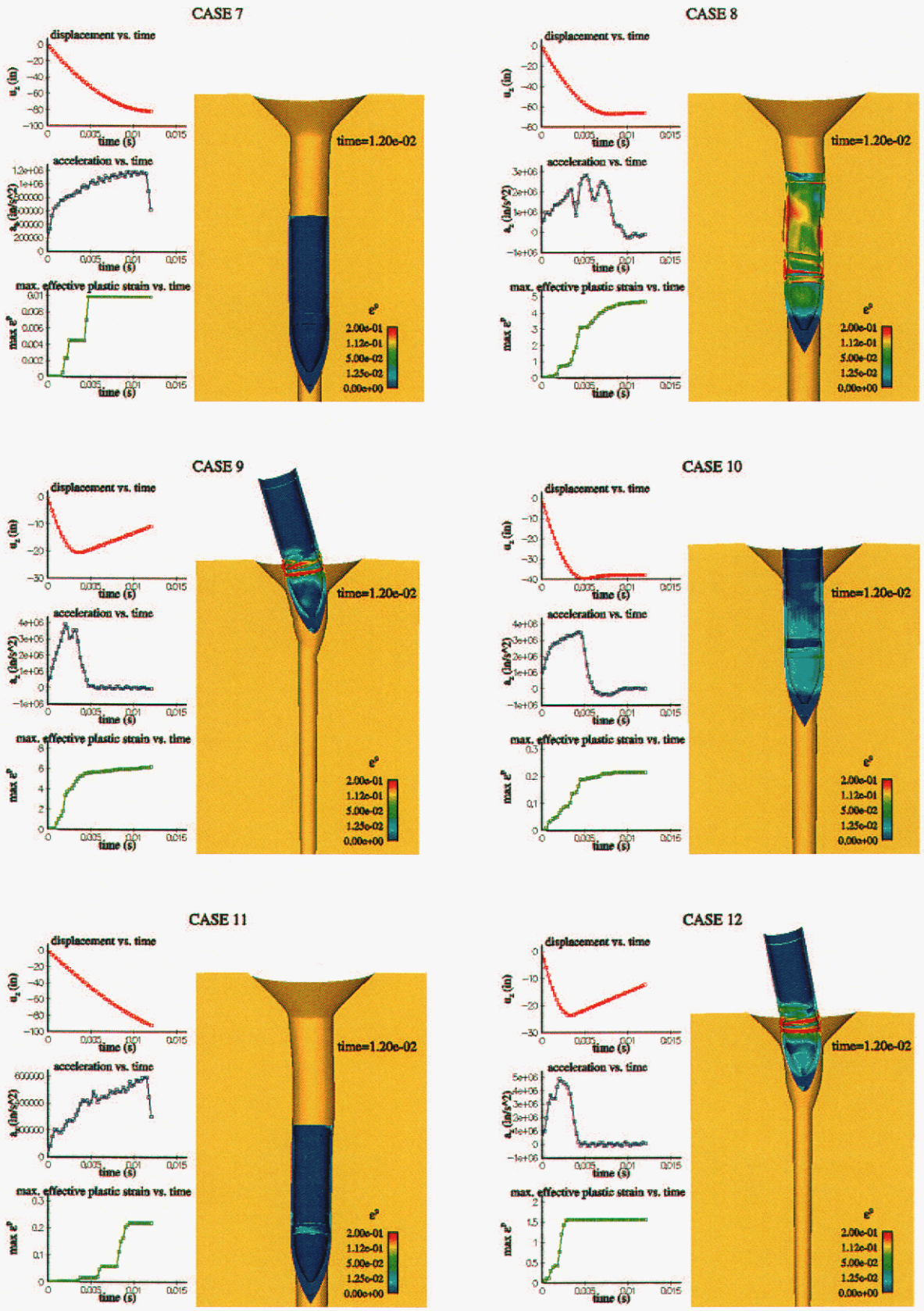

Figure 3.4: Final position of follow through penetrator and time history of displacement, acceleration and maximum effective plastic strain during penetration event, cases 7-12.

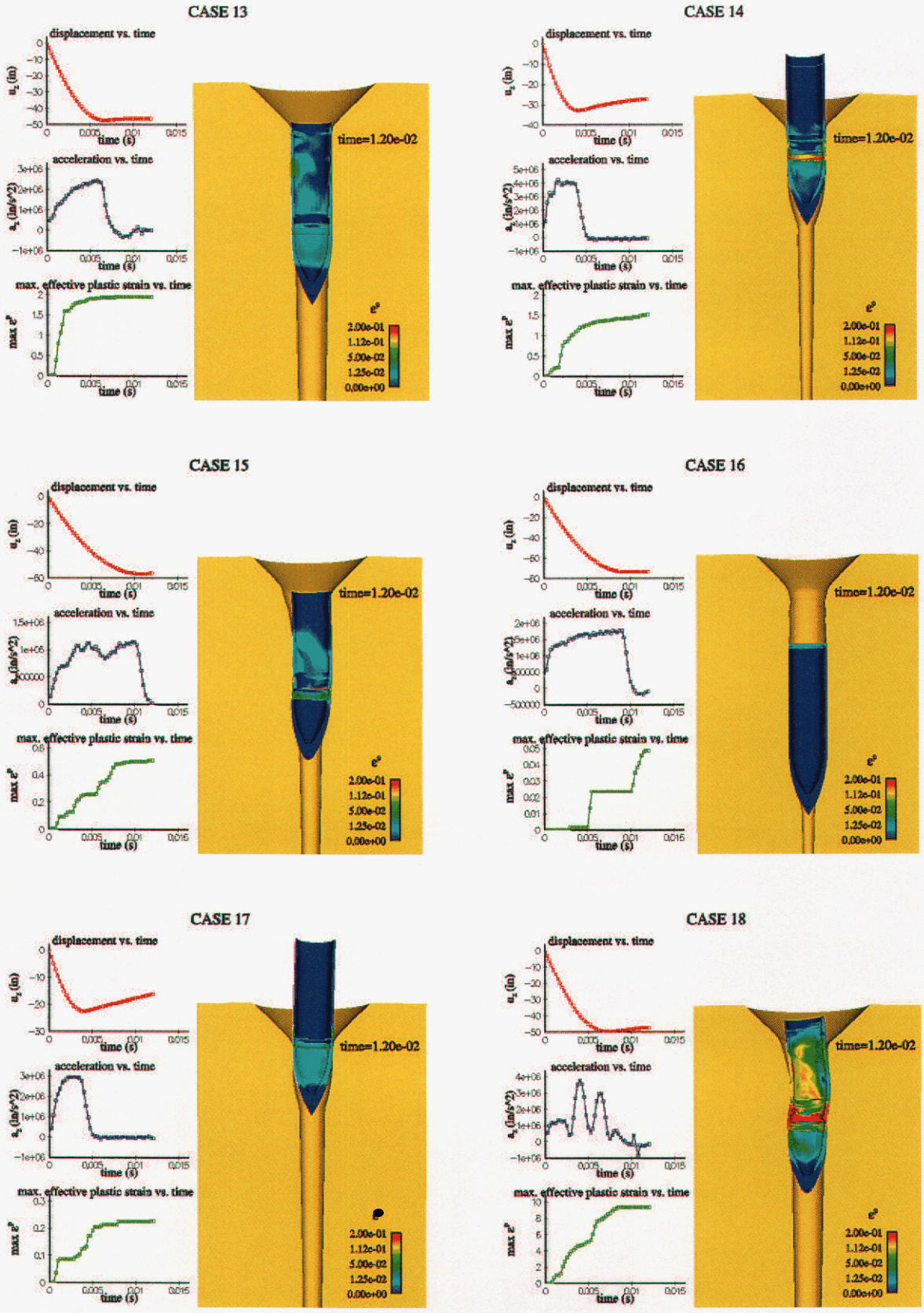

Figure 3.5: Final position of follow through penetrator and time history of displacement, acceleration and maximum effective plastic strain during penetration event, cases 13-18.

This behavior agrees with the fact that Antelope Tuff has a lower penetration resistance than CSPC and Limestone, as characterized by its lower bulk modulus and higher porosity. These results also indicate that the target material plays an important role in defining the penetration depth and penetrator deceleration.

Additional remarks can also be made regarding the maximum plastic strains induced in the penetrator case. For this metric, Figures 3.3–3.5 show that the three highest values are obtained for runs 6, 9 and 18 (average max plastic strain $\epsilon^p_{MAX} \approx 7.1$). These runs were performed using an offset of 3 in, along with the materials that have the highest resistance to peneration, CSPC (case 6) and Limestone (runs 9, 18). In these three runs the penetrator either sticks in the target (runs 6, 18) or bounces back (run 9); in either case, the penetrator does not survive the penetration process. On the other extreme, the three lowest values of ϵ^p_{MAX} occur for runs 7, 10 and 16 (average $\epsilon^p_{MAX} \approx 0.09$). These runs used an offset of 0 in, along with Tuff (run 7, 16) and Limestone (run 10) as target materials. For these three cases, the penetrator sticks in the target and survives. Note here that the highest ϵ^p_{MAX} (=0.21) is obtained for run 10 (hard target material). These remarks suggest that offset (and target material) have a strong effect on the structural integrity of the penetrator.

This initial qualitative assessment of the main effects of target material and penetrator offset is used here to summarize the time history of the normalized values of penetration depth, penetrator deceleration and maximum plastic strains for all the simulations runs. This summary is presented in Figure 3.6. From this figure, one can observe some trends regarding the response of the penetrator-target system, as briefly discussed above. Figures 3.6–A and 3.6–B show, in an average, that CSPC and Limestone produce smaller penetration depths and larger penetrator decelerations than the ones obtained for Antelope Tuff. Also, for each material, in an average, the penetration depth increases and penetrator deceleration decreases as the hole diameter increases. On the other hand, Figure 3.6–C shows a trend to obtain higher average values for the maximum plastic strains as the penetrator offset is increased. Besides, at each offset, these average values increase as the target material gets more resistance to penetration.

A summary of the normalized metrics for the maximum values of $|u_z|$, a_z, and ϵ^p, obtained from Figure 3.6, is given in Table 3.1. These values are used in the next section for performing a more formal analysis of the simulation results in order to investigate the individual or main effects of each factor as well as two-factor interactions. This investigation is based on the range of change (variation) of the metrics as the factor levels are changed (sensitivity-like studies).

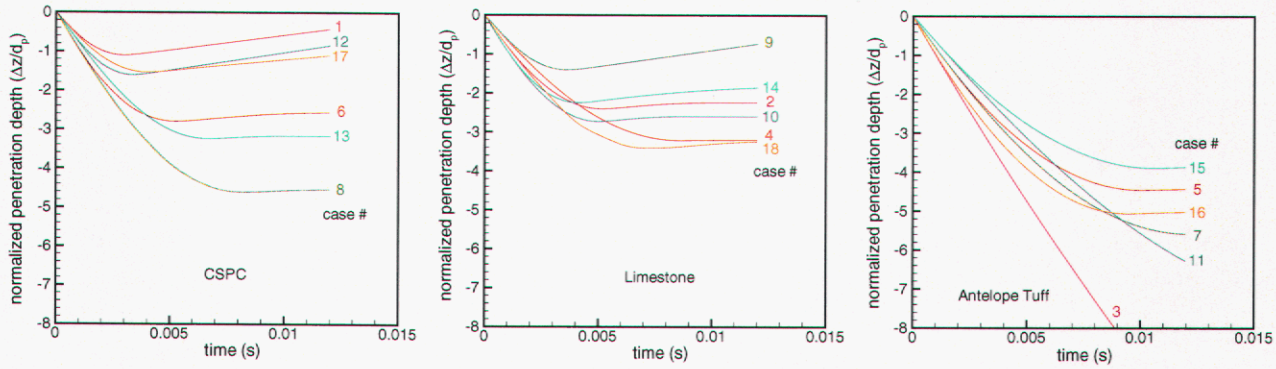

A. Normalized penetration depth $\Delta z/d_p$, $\Delta z = |u_z|$.

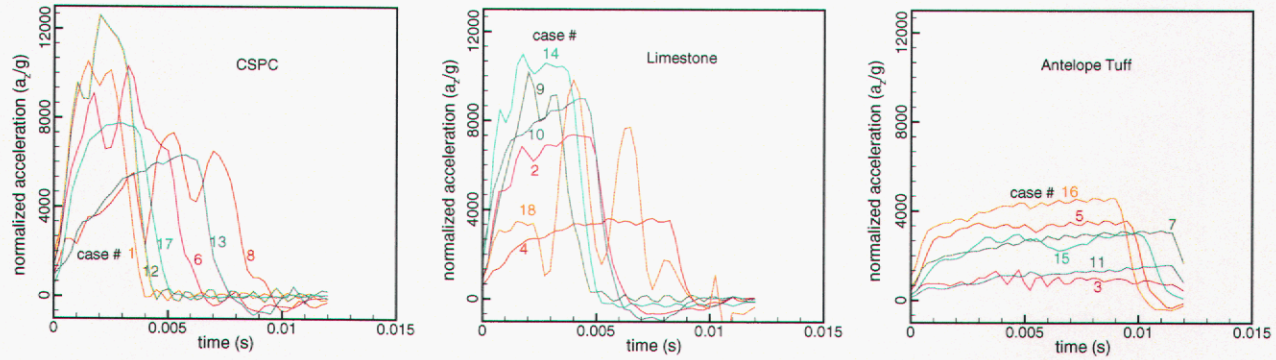

B. Normalized deceleration a_z/g.

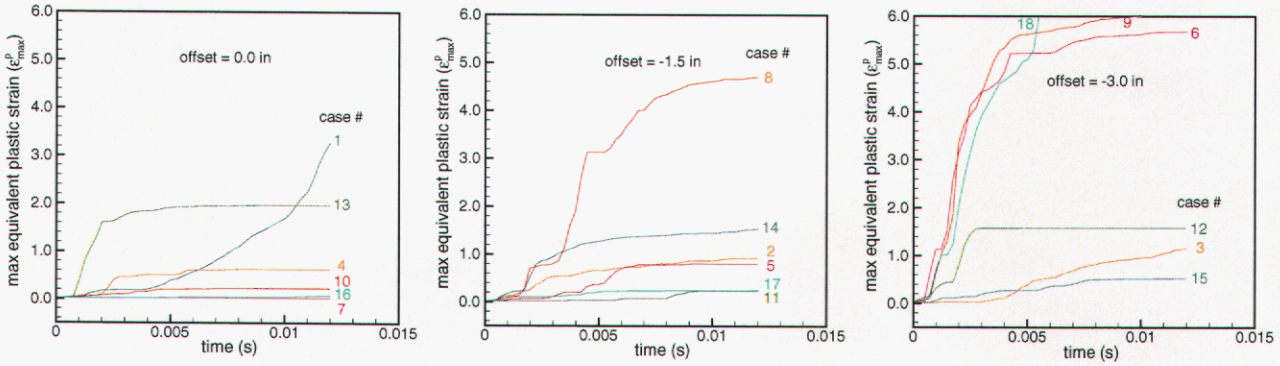

C. Maximum plastic strain ϵ^p_{MAX}.

Figure 3.6: Summary of the history of penetration depth, penetrator deceleration and maximum plastic strain in the penetrator case for the 18 simulation runs. The results are grouped based on target material (A & B) and penetrator offset (C).

Table 3.1: Performance metrics.

Run	$\frac{\lvert u_z \rvert_{MAX}}{d_p}$	$\frac{a_{zMAX}}{g}$	ϵ^p_{MAX}
1	1.11	10246.0	3.25
2	2.41	7338.5	0.91
3	14.29	1352.2	1.58
4	3.22	3579.2	0.61
5	4.46	3541.0	0.79
6	2.80	10290.0	5.66
7	5.60	3114.2	0.01
8	4.62	7305.9	4.68
9	1.42	10126.0	6.16
10	2.74	8959.8	0.21
11	7.44	1774.7	0.22
12	1.62	12566.6	1.56
13	3.25	6290.9	1.95
14	2.26	10927.6	1.52
15	3.91	2969.8	0.51
16	5.07	4544.4	0.05
17	1.55	7705.2	0.23
18	3.42	9778.9	9.32

This page intentionally left blank.

4. Effects Analysis of the Simulation Results

In this section, we carry out the analysis of the penetration event using the computed metrics shown in Table 3.1. This analysis uses graphical and statistical tools to extract the information needed to rank the selected factors based on their main/interaction effects on the outcome of the penetration process. These tools are typically used when sampling-based methodologies are applied with the DACE approach. Specifically, the tools used here are main/interaction effect plots and one-way/two-way analysis of variance (ANOVA) (Wu, *et al.*, 2000).

4.1 Study of Main Effects

The main effect of a factor is its average effect on the system response over all possible level combinations of the other factors. A main effect can be graphically represented by plotting the average value of the metrics at each factor level and connecting them by a line. These main effect plots will then illustrate the changes (variations) in the average metrics produced by a change in the factor level, and for our simulations they are displayed in Figure 4.1. In these plots, the three levels of each factor are represented on the horizontal axis with the number 0, 1, and 2, respectively (see Table 2.1). By examining these graphs, one can identify what effects might be important based on the magnitude of the induced variation in the system response, and hence, obtain a preliminary ranking of the factors effects. For example, it is clearly seen that the target material induces the greatest variation in the penetration depth and maximum deceleration, and hence, it is the most influential factor on these metrics. On the other hand, penetrator offset seems to have the stronget effect on the maximum plastic strain since the range of change of this metric is the largest. Following the same reasoning, one can then determine from these plots which is the second most important factor for each metric, then the third, and so on. To confirm this preliminary ranking, this graphical analysis is typically complemented by a formal study using statistical

tools such as analysis of variance.

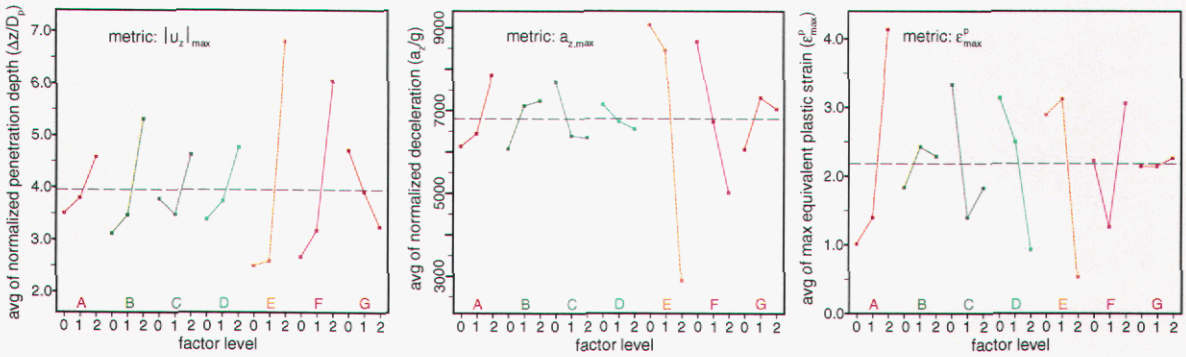

Figure 4.1: Main effects plots for $|u_z|_{MAX}$, a_{zMAX} and ϵ^p_{MAX}. The dashed line indicates the average value of the metrics over all simulation runs.

As the main effect plots, a one-way ANOVA will identify the factor subset that controls most of the output variability by detecting differences (variations) in the average value of the performance metrics when the factor levels are changed. The basic idea underlying ANOVA is the comparison of the sizes of various sums of squares of the metrics. Such comparison provides a specific test, the F–test or F–ratio (Wu, *et al.*, 2000), to detect significance of differences in the mean value of the output. This test is typically summarized in the p–value, which gives the probability that the so-called null hypothesis (i.e., that there is no differences in the means or, in other words, that there is no important effects) holds. The smaller the p–value, the stronger the evidence that the null hypothesis does not hold. In practice, a typical ANOVA study compares this computed p–value with a selected reference p–value (taken here as 0.1 or $(1-0.1)\times 100 = 90\%$ confidence) to determine whether the main effect is significant or not.

The summary of the one-way ANOVA analysis performed for each factor and for the three metrics is reported in Tables 4.1 to 4.3. Each one-way ANOVA table contains rows associated with a particular factor and the error, where the error represents all the other factor's main effects not accounted for explicitly when constructing the table. The columns are labeled "source" (of the variation), "SS for sum of squares"*, "DOF for degrees of freedom"†,

*Denote x_{ij} the jth observation (data point) at level i, $\bar{x}_{i\cdot}$ the mean of observations for the ith level, $\bar{x}_{\cdot\cdot}$ the mean of all n observations, n_i the number of observations at level i, and k the number of factor levels. Then the sums of squares for the factor and the error are defined as:

$$\mathrm{SS}_{factor} = \sum_{i=1}^{k} n_i(\bar{x}_{i\cdot} - \bar{x}_{\cdot\cdot})^2, \qquad \mathrm{SS}_{error} = \sum_{i=1}^{k}\sum_{j=1}^{n_i}(x_{ij} - \bar{x}_{i\cdot})^2, \qquad \mathrm{SS}_{factor} + \mathrm{SS}_{error} = \mathrm{SS}_{total}$$

SS_{factor} and SS_{error} are measures of the variability *between* and *within* the factor levels, respectively.

†An statistical DOF is associated with each piece of information that is estimated from the data, i.e., one allows one DOF for each independent comparison that can be made with the data.

Table 4.1: One-Way ANOVA results for maximum penetration depth, $|u_z|_{MAX}$.

source	SS	DOF	MS	F	p	PC(%)
offset	3.73	2	1.87	0.18	0.837	2.35
error	155.02	15	10.33			97.65
total	158.76	17				
vert. velocity	16.57	2	8.29	0.87	0.437	10.44
error	142.18	15	9.48			89.56
total	158.76	17				
horiz. velocity	4.22	2	2.11	0.21	0.817	2.66
error	154.53	15	10.30			97.34
total	158.76	17				
angle of attack	6.16	2	3.08	0.30	0.743	3.88
error	152.59	15	10.17			96.12
total	158.76	17				
target material	72.61	2	36.31	6.32	0.010	45.74
error	86.14	15	5.74			54.26
total	158.76	17				
hole diameter	39.91	2	19.96	2.52	0.114	25.14
error	118.85	15	7.92			74.86
total	158.76	17				
hole taper	6.52	2	3.26	0.32	0.730	4.11
error	152.24	15	10.15			95.89
total	158.76	17				

"MS for mean squares" ($\text{MS} = \text{SS}_{source}/\text{DOF}_{source}$), "F for F–ratio" ($\text{F} = \text{MS}_{factor}/\text{MS}_{error}$), and "p for p–value or probability". Note that only the row corresponding to a factor has a probability associated with it. The tables have been extended to include an additional column representing the percentage contribution (PC) which is the ratio $\text{PC} = \text{SS}_{source}/\text{SS}_{total}$. As indicated by its definition, PC gives a quantitative measure of how much of the total variation is attributed to each factor, and hence, it indicates the relative power of a factor to reduce variation. It can be used, along with the p–value, to assess the relative importance of each factor effect on the response. For example, consider the ANOVA results for the metric $|u_z|_{MAX}$ (penetration depth) and for the factor target material, Table 4.1. Focusing on the values located in the p–value and PC columns, we can affirm that with a $(1-\text{p}) \times 100 = 99\%$ confidence (which is greater than the 90% reference value) that the target material has a significant main effect on the penetration depth (null hypothesis does not hold), and that its contribution to the total variation of this metric is about 46%. Following a similar analysis

for each factor, one can then obtain a ranking using these objective measures of statistical significance.

Table 4.2: One-Way ANOVA results for maximum decelerarion, a_{zMAX}.

source	SS	DOF	MS	F	p	PC(%)
offset	10147263	2	5073631	0.38	0.690	4.84
error	199695013	15	13313001			95.16
total	209842276	17				
vert. velocity	4892885	2	2446442	0.18	0.838	2.33
error	204949391	15	13663293			97.67
total	209842276	17				
horiz. velocity	7105562	2	3552781	0.26	0.772	3.39
error	202736714	15	13515781			96.61
total	209842276	17				
angle of attack	1102255	2	551128	0.04	0.961	0.53
error	208740021	15	13916001			99.47
total	209842276	17				
target material	139287168	2	69643584	14.81	0.000	66.38
error	70555108	15	4703674			33.62
total	209842276	17				
hole diameter	39902530	2	19951265	1.76	0.206	19.02
error	169939746	15	11329316			80.98
total	209842276	17				
hole taper	5186998	2	2593499	0.19	0.829	2.47
error	204655278	15	13643685			97.53
total	209842276	17				

The ranking of the factors obtained from the ANOVA Tables is presented in Table 4.4. The computed percentage contributions are also listed in the table for reference. Note that this table confirms the conclusion obtained from the main effect plots that the target material and hole diameter are the most influencial factors for maximum penetration depth and maximum deceleration, while penetrator offset and target material have the strongest effect on the maximum plastic strain of the penetrator case. Note that the percentage contribution of the factors for the three metrics add up to 94.32%, 98.96% and 84.07%, respectively, meaning that the 7 selected factors account for most of the variation in the responses of the penetrator-target system.

Table 4.3: One-Way ANOVA results for maximum plastic strain, ϵ^p_{MAX}.

source	SS	DOF	MS	F	p	PC(%)
offset	34.73	2	17.37	3.16	0.072	29.63
error	82.49	15	5.50			70.37
total	117.23	17				
vert. velocity	1.16	2	0.58	0.07	0.928	0.99
error	116.07	15	7.74			99.01
total	117.23	17				
horiz. velocity	12.50	2	6.25	0.90	0.429	10.66
error	104.73	15	6.98			89.34
total	117.23	17				
angle of attack	15.55	2	7.78	1.15	0.344	13.26
error	101.68	15	6.78			86.74
total	117.23	17				
target material	24.76	2	12.38	2.01	0.169	21.12
error	92.47	15	6.16			78.88
total	117.23	17				
hole diameter	9.80	2	4.90	0.68	0.520	8.36
error	107.43	15	7.16			91.64
total	117.23	17				
hole taper	0.06	2	0.03	0.00	0.996	0.05
error	117.17	15	7.81			99.95
total	117.23	17				

Table 4.4: Ranking of factor's main effects based on metrics.

rank	$\lvert u_z \rvert_{MAX}$ factor	PC(%)	a_{zMAX} factor	PC(%)	ϵ^p_{MAX} factor	PC(%)
1	target material	45.74	target material	66.38	offset	29.63
2	hole diameter	25.14	hole diameter	19.02	target material	21.12
3	vert. velocity	10.44	offset	4.84	angle of attack	13.26
4	hole taper	4.11	horiz. velocity	3.39	horiz. velocity	10.66
5	angle of attack	3.88	hole taper	2.47	hole diameter	8.36
6	horiz. velocity	2.66	vert. velocity	2.33	vert. velocity	0.99
7	offset	2.35	angle of attack	0.53	hole taper	0.05

4.2 Study of Two-Factor Interaction Effects

Because the interpretation of individual effects of factors that are involved in significant higher-order interactions may not be appropriate, it is important, when possible, to complement the main effects study with an interaction effects analysis. By interaction effects we mean that the effect of a factor can be distinct at different levels of the other factors. Interaction effects can be important for nonlinear problems, where the factor's effects are not additive. In this work, we are able to study mainly two-factor interactions due to the characteristics of the selected orthogonal array (strength 2). Higher-order interactions can not be extracted using this array since they are confounded with other effects.

A two-factor interaction can be graphically represented using interaction plots. Similar to the main effects plots, interaction plots are constructed using the mean value of the response, with the means, in this case, computed for each combination of levels of the 2 factors. No interaction between the factors is present if the resulting connecting lines are parallel. The greater the lines depart from being parallel, the stronger the degree of interaction. For the present numerical experiment, the 7 selected factors will give 21 two-factor interaction plots for each metric. Three of these plots per metric, represented in an interaction-plot matrix, are depicted in Figures 4.2 to 4.4. Each matrix considers the first three factors that have the most effect on each of the response metrics (see Table 4.4). In these two-factor interaction plots, obtained using the MINITAB statistical software (Minitab Inc.), the factors are represented by the letters C1 (offset), C2 (vertical velocity), C4 (angle of attack), C5 (target material) and C6 (hole diameter), with the corresponding levels indicated by the numbers 0, 1 and 2 (see Table 2.1). The horizontal axis in each plot or matrix panel indicates the level of factor 1 while the vertical axis gives the mean value of the metric. Each of the 3 plotted lines in each panel then shows the penetrator-target response at each level of factor 2. Note that in the interaction plot matrix, each pair of factors provides two panels, i.e., they show "factor 1 by factor 2" and "factor 2 by factor 1". From these plots it is observed that there exist interactions between the factors since the lines show deviations from being parallel, although such deviations are small for some cases (e.g. see C5 vs C6 or C6 vs C5 for $|a_z|_{MAX}$). The greater degree of interaction corresponds to the parameters affecting ϵ^p_{MAX}. In the other cases, the degree of interactions is smaller. As before, to confirm that this observed behavior is statistically significant, one must follow up this graphical analysis with an ANOVA study.

A two-way ANOVA takes two factors at a time to construct the corresponding ANOVA table. As mentioned before, the basic idea of this analysis is to test the statistically significance of an effect by computing specific sum of squares of the response metrics. This computation gives the F–ratio and the corresponding p–value. By comparing this computed p–value with a reference p–value (taken here as 0.1 - 90% confidence), one could determine the significance of the interaction effect. Tables 4.5 to 4.7 summarize the ANOVA computations for the three metrics using the first three main factors from Table 4.4. The rows in

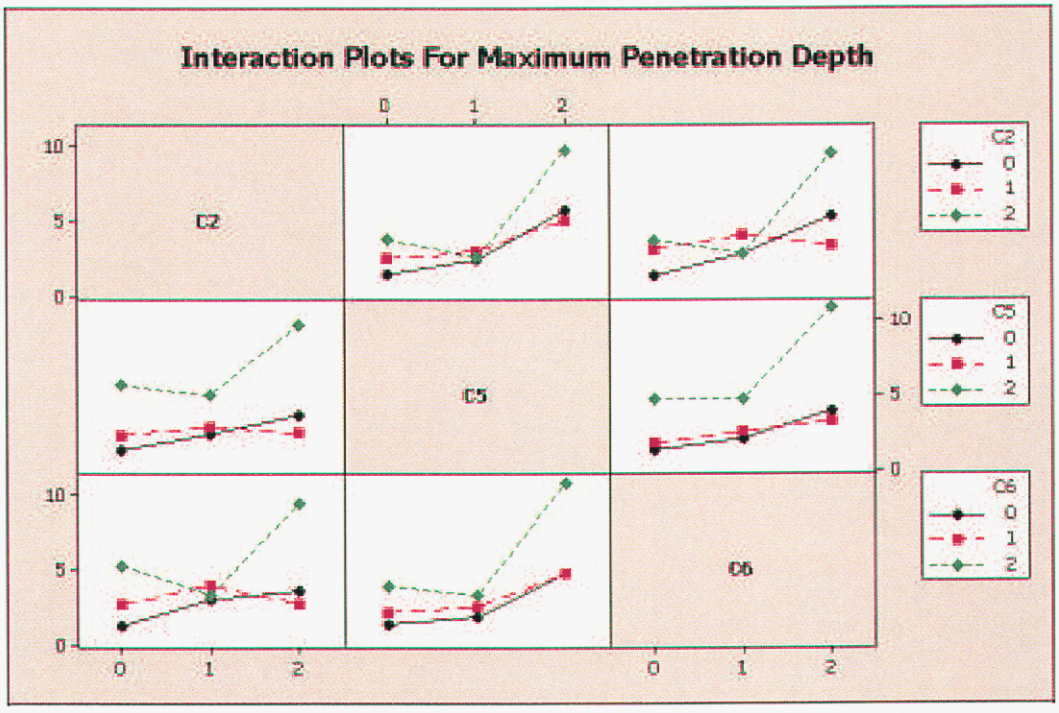

Figure 4.2: Interaction plots for maximum penetration depth, $|u_z|_{MAX}$.

Table 4.5: Two-Way ANOVA Tables. Metric: $|u_z|_{MAX}$.

source	SS	DOF	MS	F	p	PC(%)
target material	72.61	2	36.31	11.95	0.003 |	
hole diameter	39.91	2	19.96	6.57	0.017 ⟩	82.77
interaction	18.88	4	4.72	1.55	0.267 |	
error	27.35	9	3.04			17.23
total	158.76	17				
target material	72.61	2	36.31	5.97	0.022 |	
vert. velocity	16.57	2	8.29	1.36	0.304 ⟩	65.54
interaction	14.86	4	3.72	0.61	0.665 |	
error	54.71	9	6.08			34.46
total	158.76	17				
hole diameter	39.91	2	19.96	2.51	0.136 |	
vert. velocity	16.57	2	8.29	1.04	0.392 ⟩	54.92
interaction	30.70	4	7.67	0.96	0.472 |	
error	71.58	9	7.95			45.09
total	158.76	17				

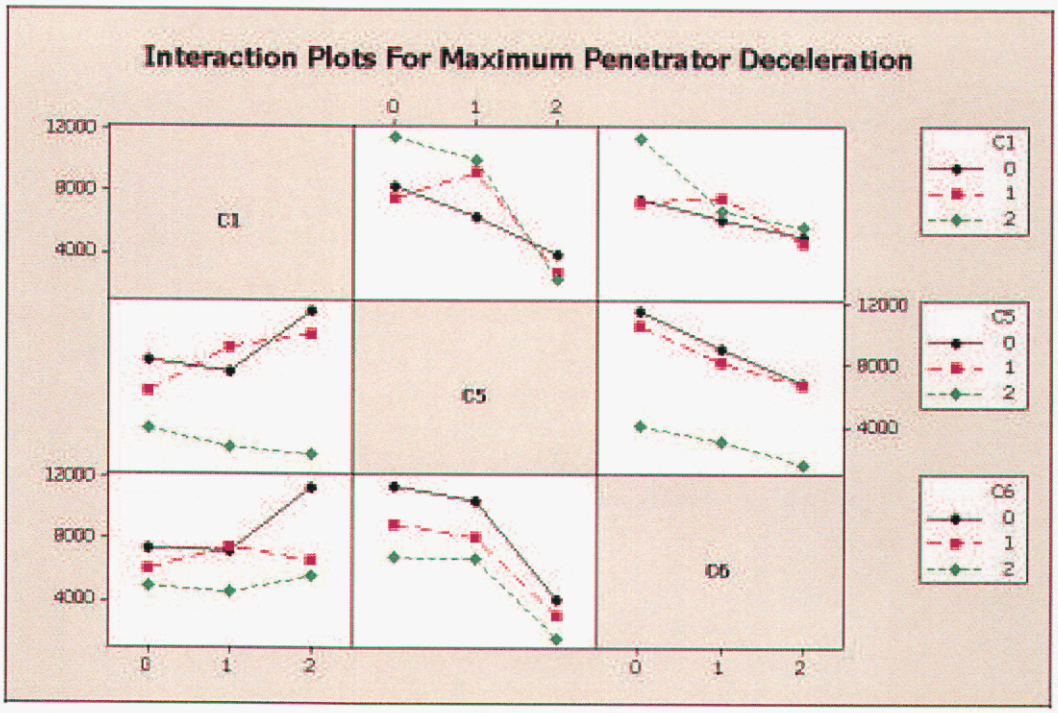

Figure 4.3: Interaction plots for maximum deceleration, a_{zMAX}.

Table 4.6: Two-Way ANOVA Tables. Metric: a_{zMAX}.

source	SS	DOF	MS	F	p	PC(%)
target material	139287168	2	69643584	22.38	0.000 |	
hole diameter	39902530	2	19951265	6.41	0.019 ⟩	86.66
interaction	2647201	4	661800	0.21	0.925 |	
error	28005377	9	3111709			13.35
total	209842276	17				
target material	139287168	2	69643584	17.73	0.001 |	
offset	10147263	2	5073631	1.29	0.321 ⟩	83.16
interaction	25048090	4	6262022	1.59	0.257 |	
error	28005377	9	3111709			16.85
total	209842276	17				
hole diameter	39902530	2	19951265	1.24	0.335 |	
offset	10147263	2	5073631	0.32	0.737 ⟩	30.94
interaction	14854034	4	3713509	0.23	0.914 |	
error	28005377	9	3111709			69.07
total	209842276	17				

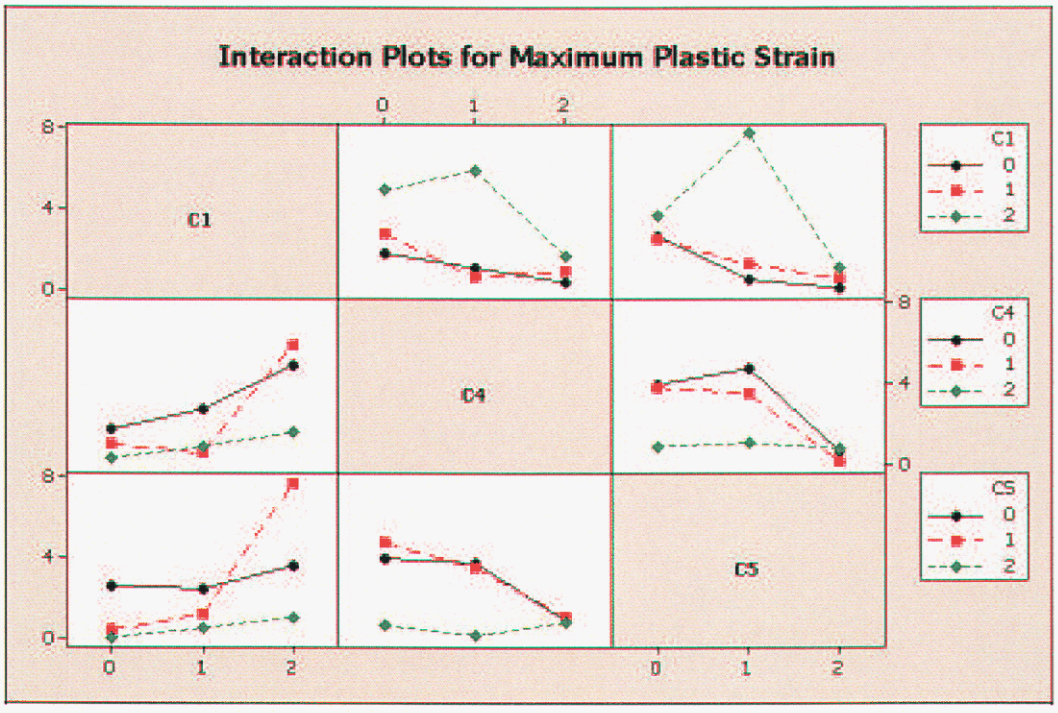

Figure 4.4: Interaction plots for maximum plastic strain, ϵ^p_{MAX}.

Table 4.7: Two-Way ANOVA Tables. Metric: ϵ^p_{MAX}.

source	SS	DOF	MS	F	p	PC(%)
offset	34.73	2	17.37	6.20	0.020 |	
target material	24.76	2	12.38	4.42	0.046 ⟩	78.48
interaction	32.50	4	8.13	2.90	0.085 |	
error	25.23	9	2.80			21.52
total	117.23	17				
offset	34.73	2	17.37	2.88	0.108 |	
angle of attack	15.55	2	7.78	1.29	0.322 ⟩	53.71
interaction	12.69	4	3.17	0.53	0.720 |	
error	54.27	9	6.03			46.28
total	117.23	17				
angle of attack	15.55	2	7.78	1.06	0.385 |	
target material	24.76	2	12.38	1.69	0.237 ⟩	43.89
interaction	11.15	4	2.79	0.38	0.817 |	
error	65.77	9	7.31			56.10
total	117.23	17				

these tables are now associated with each of the two factors, their interaction and the error, while the columns are similar to the ones previously used for the one-way ANOVA. Here, the column for percentage contribution now indicates the total effect of the two factors, i.e., their main effects and corresponding interaction.

Consider first Tables 4.5 and 4.6. Based on the computed p–value, it is observed that interaction effects between the three main factors defining the maximum penetration depth, $|u_z|_{MAX}$, and maximum deceleration, a_{zMAX}, are not significant. The level of confidence to suggest the presence of the interactions for these factors ranges from 74.3% (p=0.257: target material–offset for a_{zMAX}) to 7.5% (p=0.925: target material–hole diameter for a_{zMAX}), which are pretty low compared to the reference value of 90%. Hence, it is adequate to consider the individual effects of these factors alone when analyzing penetration events with regard to these two metrics. Note that Tables 4.5 and 4.6 re-affirm the fact that target material and hole diameter are the most important factors for these metrics, accounting for 82.77% and 86.66% of the variation in the response of $|u_z|_{MAX}$ and a_{zMAX}, respectively.

Next, consider the maximum plastic strain, Table 4.7. This table shows that, besides having a strong individual effect, both offset and target material interact significantly (p=0.085 or 91.5% confidence) to produce the response variation in ϵ^p_{MAX}. These two factors together could account for 78.48% of such variation. Regarding the other two-factor interactions, they seem to be weak due to their low level of confidence (28% and 18.3%, respectively). Therefore, Table 4.7 seems to suggest that penetration studies focusing on the structural integrity of the penetrator should account for not only the individual effects but also the coupled effects of both offset and target material.

5. Discussion of the Simulation Results – OAT Analysis

The DACE approach used in this screening study has proven very useful to rank the importance of the input factors (parameters) affecting the outcome of the penetration process. As seen, the approach gives a suitable mathematical framework consisting of sampling-based methodologies and statistically-based (variance-based) techniques to evaluate the factor effects on a particular model response. This approach leads to statistically justified conclusions which are very general since each factor effect, evaluated at different levels of the other factors, describes its main effect and possible interaction with other factors. Factor interactions are typically present in highly nonlinear models such as the penetrator-target system.

The three factors identified by the present DACE study as the most influencial for the penetration event are target material, hole diameter, and penetrator offset. The first two have significant effects on the penetration depth and maximum deceleration loads, while the second and third ones are the most influencial for the structural response of the penetrator (maximum plastic strain). Only penetrator offset and target material show a strong two-factor interaction, meaning that the effect of offset on plastic strain depends on the specific target material used, and viceversa. Since the interaction effects of target material and hole diameter are small, the main effect of one does weakly depend on the level of the other.

Due to the computational size of the problem and time limitations, other factors such as geometry of the penetrator (length, diameter, weight) and the friction coefficient (μ) at the interface penetrator-target, were not included in the present DACE study. Some of these factors have been considered in other studies. In particular, Chen, 1989, evaluated the impact of the friction coefficient on the standard penetration process of geological targets (without a preformed hole) using one-factor-at-a-time (OAT) numerical experiments, and found out that an effect of this parameter was present. Recall that OAT studies evaluate first order (main) effects by changing the values of each factor in turn, and hence they do not capture interaction effects.

To obtain an insight of the relative importance of the friction coefficient (μ) for pen-

etration events, we decided to carry out a three-level OAT analysis involving the friction coefficient and the three main factors mentioned above: target material, hole diameter, and penetrator offset. This analysis is mainly performed in a qualitative fashion by comparing graphically the magnitude of the induced change in the time history of a particular model response as the factor level is varied. The selected responses are again penetration depth, penetrator deceleration and maximum plastic strain in the penetrator case. For this study, we take as reference (nominal) configuration of the penetrator-target model the following values: $\mu = 0.04$, offset = 0 in, $V_V = 1000$ ft/s, $V_H = 0$ ft/s, $\alpha = 0^o$, Limestone, $d_h = 10$ in, $\beta = 0^o$ (obliquity = 0^o). The levels of offset, target material, and hole diameter are varied one-at-a-time from their nominal values using the levels given in Table 2.1. The upper and lower limits for μ are taken as 0.0 and 0.08 (Chen, 1989), respectively.

The summary of the OAT simulation runs is presented in Figures 5.1 to 5.3. Each figure displays the effect of each factor on the time history of $|u_z|$, a_z and ϵ^p_{MAX}, as the factor level is varied one at a time. Based on the range of the induced variation of $|u_z|$ and a_z, Figures 5.1 and 5.2 suggest the following order of importance of the factors for these responses: target material, hole diameter, friction coefficient and offset. It is clear from these figures that (i) offset has a small effect on these metrics, an aspect that agrees well with the DACE ranking of the factors, Table 4.4, and (ii) CSPC and Limestone show effects that are close to each other due to the similar penetration resistance of both materials. Note that the interaction of friction with the other factors are not accounted for in these figures, and hence, the effects illustrated in Figures 5.1 and 5.2 may be altered if the values of the friction coefficient are changed simultaneously with the other factor levels. With regard to ϵ^p_{MAX}, Figure 5.3 seems to indicate that the order of importance of the factors is: offset, friction, hole diameter and target material. Note that the order of the last two factors (hole diameter and target material) is opposite to the order found in the DACE study. However, one has to keep in mind that target material and offset interact strongly, and hence the effect of target material is being greatly influenced by the specific value of offset. Accounting for this interaction, the order of these two factors should be switched. Also, the jump in ϵ^p_{MAX} observed in Figure 5.3–D when $\mu = 0.08$ is due to the restricted rebound of the penetrator from the elastic unloading of the target once the penetrator velocity is reduced to zero. This induced higher deformations imposed by the target material when friction is increased suggest a coupling between these two factors. When these interactions are accounted for explicitly, this coupling and other factor's couplings with friction will be manifested in their main effects, Figure 5.3.

Previous parametric studies of the penetration event have typically used OAT approaches to investigate how the penetration depth and penetrator deceleration are affected by specific factors, such as hole diameter and impact velocity. For pilot-hole assisted penetration studies, in particular, Andersen, 2004, has observed an increased penetration depth and a decreased deceleration when the hole diameter is $d_h/d_p \geq 0.7$. The present study has partially validated these findings, as shown in Figures 5.4–5.5. Figure 5.4–A presents the average value of

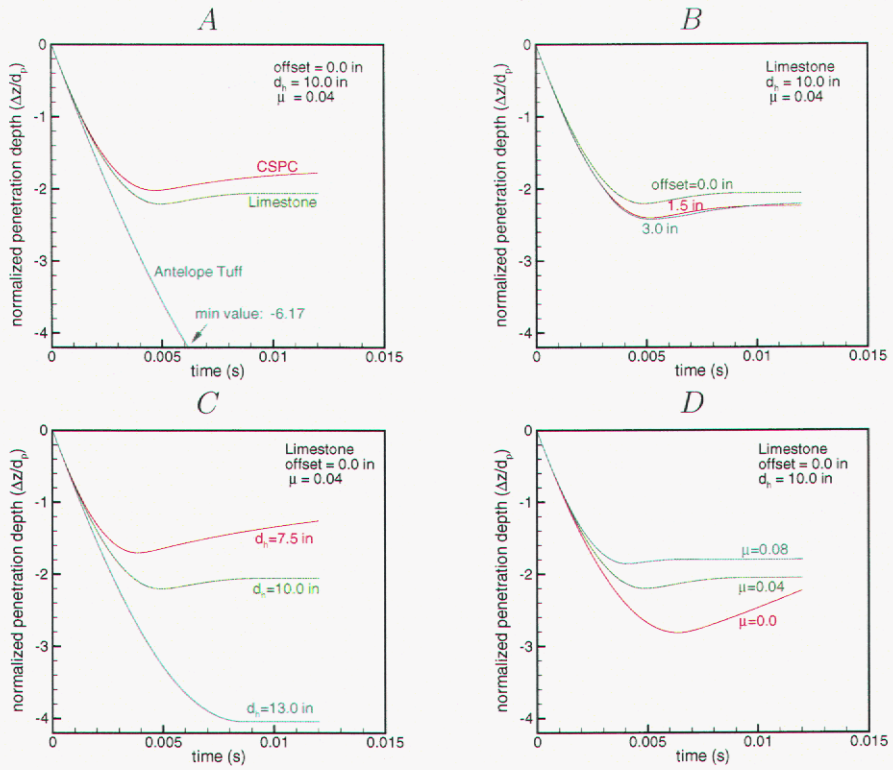

Figure 5.1: OAT studies: effect of (A) target material, (B) offset, (C) hole diameter, d_h, and (D) friction coefficient, μ, on penetration depth.

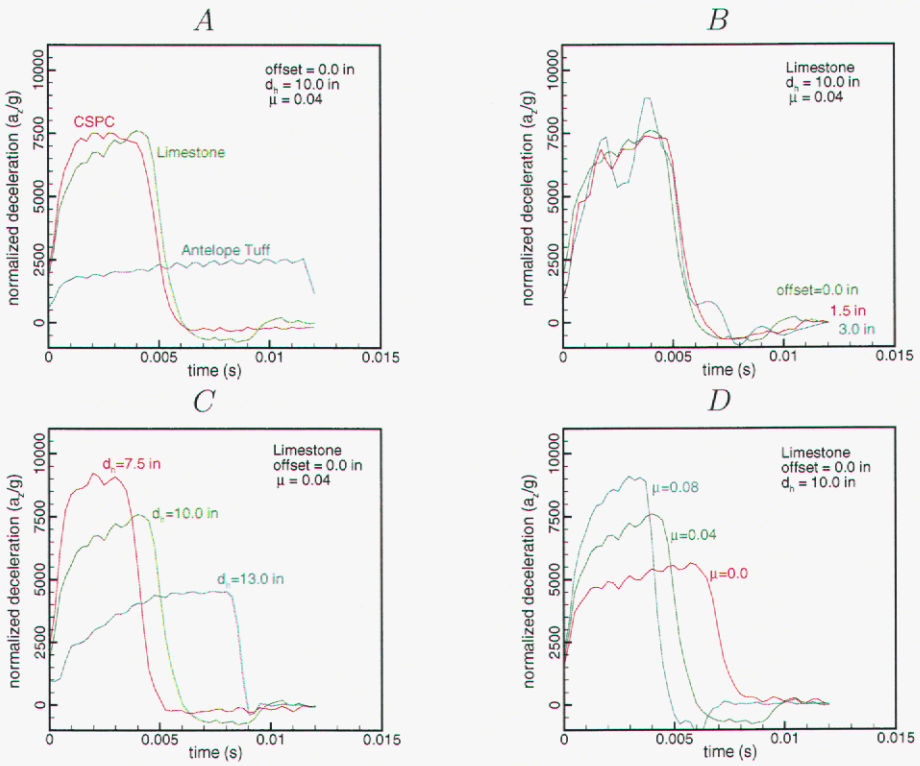

Figure 5.2: OAT studies: effect of (A) target material, (B) offset, (C) hole diameter, d_h, and (D) friction coefficient, μ, on penetrator deceleration.

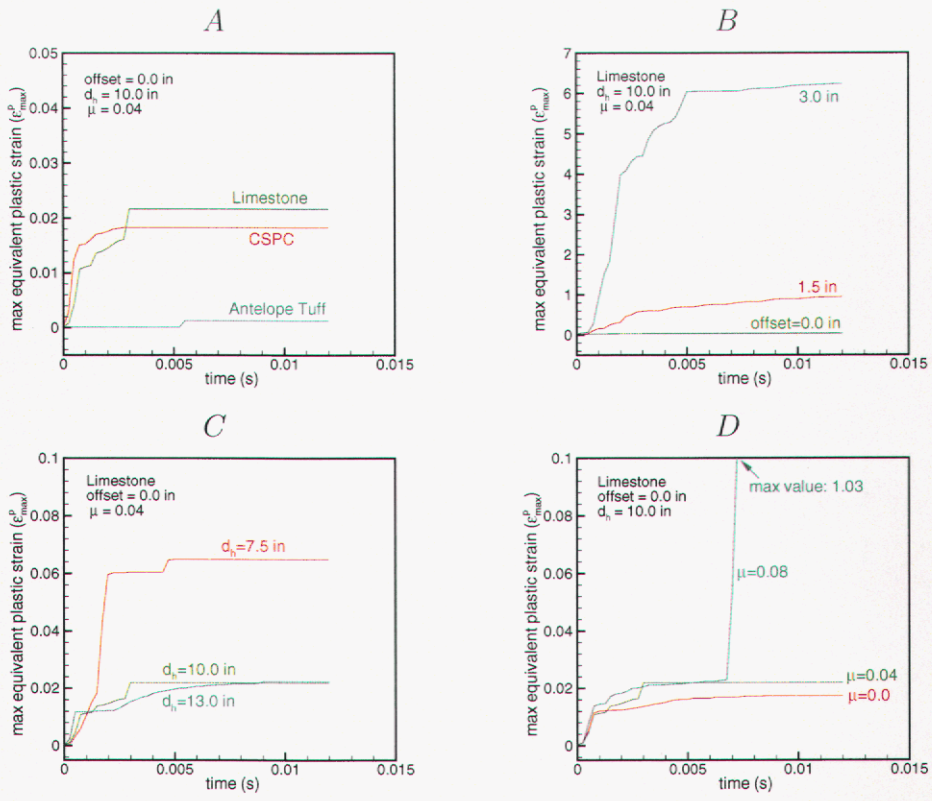

Figure 5.3: OAT studies: effect of (A) target material, (B) offset, (C) hole diameter, d_h, and (D) friction coefficient, μ, on maximum plastic strain.

$|u_z|_{MAX}/d_h$ as a function of d_h/d_p for each target material (solid line) computed using the values from Table 3.1 (DACE results). Recall that these results are obtained from simulations where all the factors are varied at the same time. In the same figure, the dashed line displays the average behavior of $|u_z|_{MAX}$ over the three target materials. One can observe that the target material has a strong effect on the induced increase (rate) of penetration depth as the diameter of the hole increases. Is it noticeable that, for $d_h/d_p \geq 0.7$, this rate can increase (Tuff), slightly decrease (Limestone) or be almost constant (CSPC), a type of response that in general does not follow the expected trend. However, the average response smooths out these differences, reproducing the trend observed by Andersen, 2004.

Figure 5.4–B shows a comparison of the curves $|u_z|_{MAX}/d_h$ versus d_h/d_p obtained with the DACE study (average) and the one obtained from the OAT analysis. Similar to the trend obtained for the average response, the computed OAT values give an increased penetration depth as the hole diameter increases beyond $d_h/d_p \approx 0.7$. It is important to note here that the trends obtained for the same material (Limestone), computed with both DACE (Figure 5.4–A) and OAT (Figure 5.4–B) approaches, are not quite the same. In fact, the rate obtained

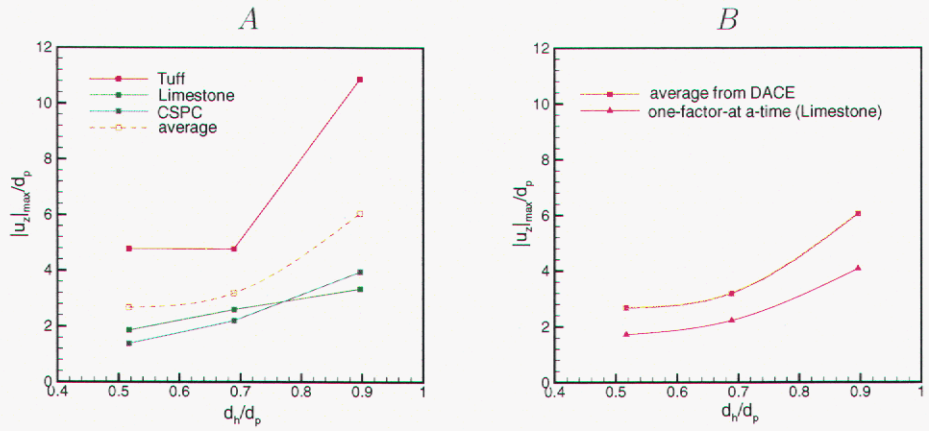

Figure 5.4: Maximum penetration depth as a function of hole diameter.

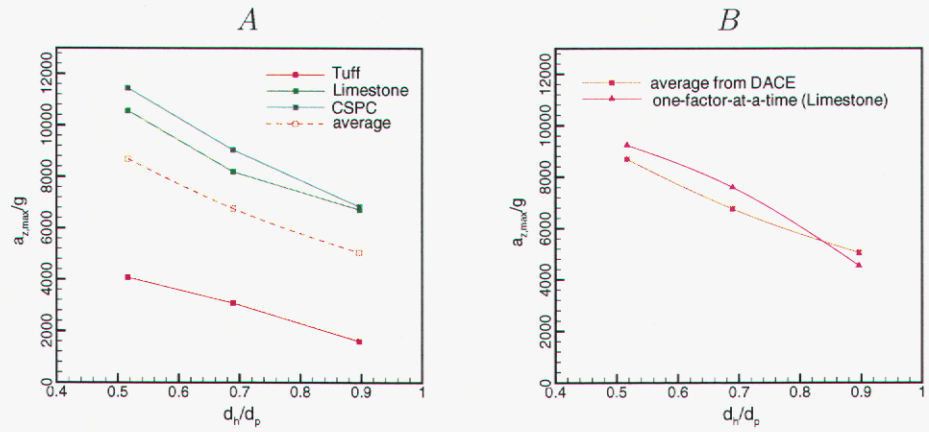

Figure 5.5: Maximum deceleration of penetrator as a function of hole diameter.

from the DACE approach slightly decreases after $d_h/d_p \approx 0.7$, while the corresponding rate computed from the OAT study increases. This difference in response is due to the presence of combined effects (interactions) among the different factors used in the DACE study, effects that although small (see Figure 4.5), add up to affect the overall response. By its nature, the OAT approach can not capture these interaction effects.

Figure 5.5–A displays the curves a_{zMAX}/g versus d_h/d_p for each target material from the DACE analysis (solid line) and for average response (dashed line), while Figure 5.5–B compares similar curves for the average behavior (DACE) and for the response obtained using the OAT method. The trend observed by Andersen, 2004, with regard to a decreased maximum deceleration for $d_h/d_p \geq 0.7$ is not reproduced, in general, by the DACE approach (presence of interaction effects); however such trend is obtained from the OAT analysis.

As mentioned before, the follow through penetration concept relies on the formation of a precursor hole in the target material to aid the penetration event. It has been observed (Baty, *et al.*, 2003; Vigil, 2003), and confirmed in these studies, that the creation of such a hole with an adequate diameter produces deeper penetration depths (penetrator sticks in target; see Figures 3.6–A, 5.1–C), and substantially reduces the deceleration loads (penetrator survives; see Figures 3.6–B, 5.2–C). The use of a preconditioned target, then, increases the chances for a succesful penetration event. Note here that the presence of a pilot hole also avoids rebounds from penetration resistant (hard) targets, as can be observed from Figure 5.6. This figure shows the final position of the penetrator for penetration events modeled using $d_h = 13, 10, 7.5, 5, 2$ in. and Limestone as target material (a hard target). The other parameters are set to: offset = 0 in, $V_V = 1000$ ft/s, $V_H = 0$ ft/s, $\alpha = 0^o$, $\beta = 0^o$ and $\mu = 0.04$. From this figure it is clearly seen that the possibility of a rebound from the hard target increases as the size of the hole decreases (the limit being a penetration process without a pilot hole). It seems that the rebound is less probable for $d_h/d_p \geq 0.7$. Typically, this rebound is accompanied by very high deceleration loads and large plastic strains in the penetrator case that could damage the penetrator and its internal components.

A side effect brought about by the presence of the pilot hole is the possibility of the misalignment or offset from the hole centerline that is prejudicial to the structural integrity of the penetrator. This is particularly important when hard target materials are involved in the penetration event. The amount of offset that the follow through penetrator experiences is a combined effect of both (i) the magnitude of the angle of attack of the penetrator and (ii) the time passed between precursor shaped charge detonation, at a given standoff above the target surface, and the impact of the penetrator on the preconditioned target. Note here that the shaped charge tip can have a velocity two orders of magnitude greater than the penetrator, which remains at the velocity and trajectory of the delivery vehicle.

To appreciate the effect of an offset on the structural response of the penetrator, Figure 5.7 presents the final position of the penetrator obtained during a penetration event simulated using Limestone as target material and offsets of 0.0 in, 1.5 in, 3.0 in and 4.5 in (ratios of $offset/r_h = 0, 0.3, 0.6, 0.9$; $d_h = 2r_h = 10$ in). The other factors are set to the values $V_H = 1000$ ft/s, $V_V = 0$ ft/s, $\alpha = 0^o$, $\beta = 0^o$ and $\mu = 0.04$. One can observe from the contour plots for plastic strain shown in this figure that the state of the penetrator deformation gets more severe with an increasing offset. This highly deformed state is mainly localized to areas close to the joint of the penetrator's case-nose, and starts to spread out as the offset increases. The magnitude of the maximum plastic strains induced in the penetrator is summarized in Figure 5.8. Figure 5.8–A shows the computed ϵ^p_{MAX} vs offset/r_h curve for each material used in the DACE study, while Figure 5.8–B presents similar curves obtained from both the OAT study (except the case for offset/$r_h = 0.9$) and the average values from the DACE analysis. Both figures show the same trends, i.e., an increased maximum plastic strain as the offset is increased. This figure also seems to indicate that, in general, values of offset/r_h greater than 0.3 should be avoided to increase the possibility of penetrator survival during the penetration

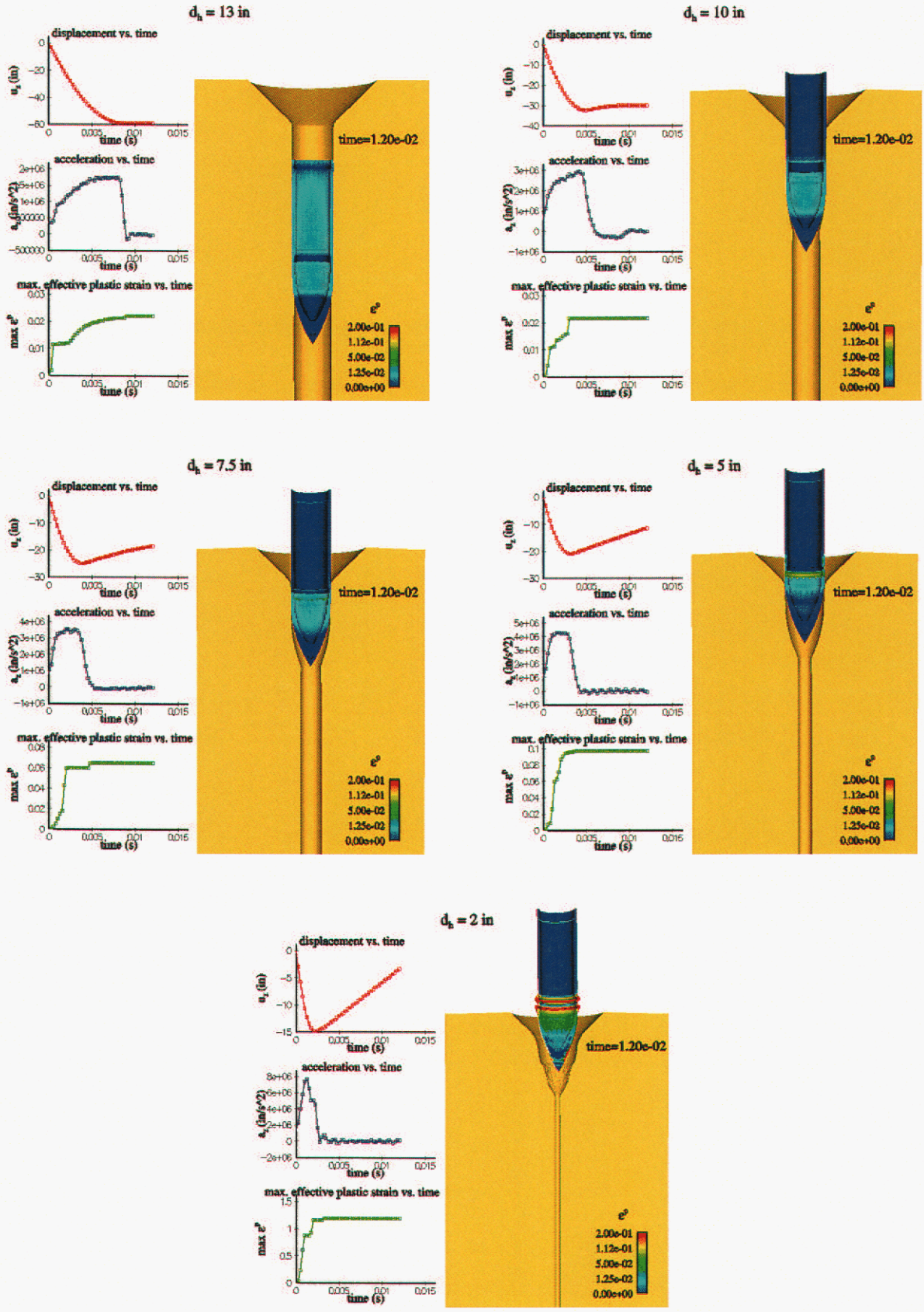

Figure 5.6: Effect of hole diameter on penetration event.

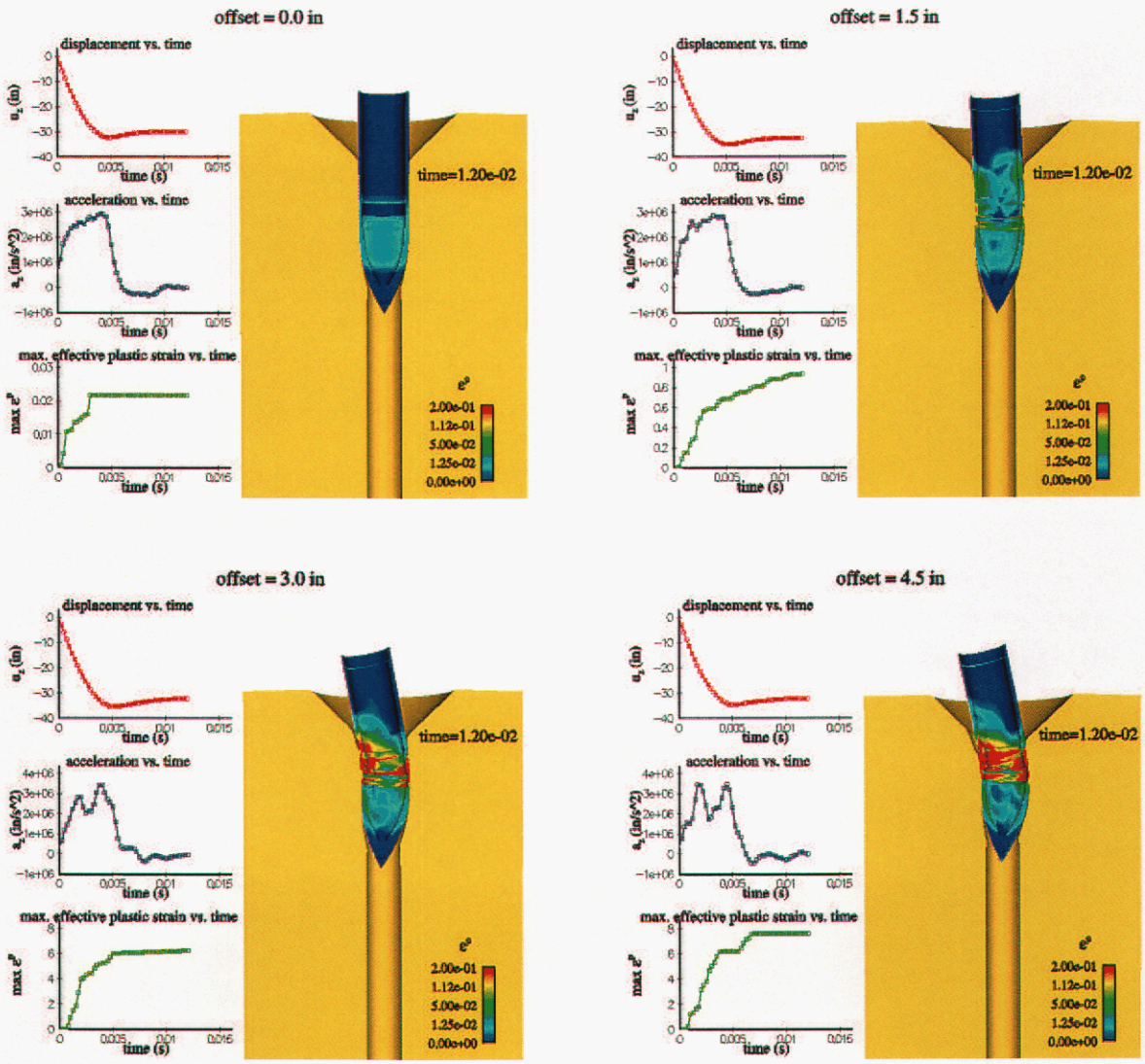

Figure 5.7: Effect of offset on penetration event.

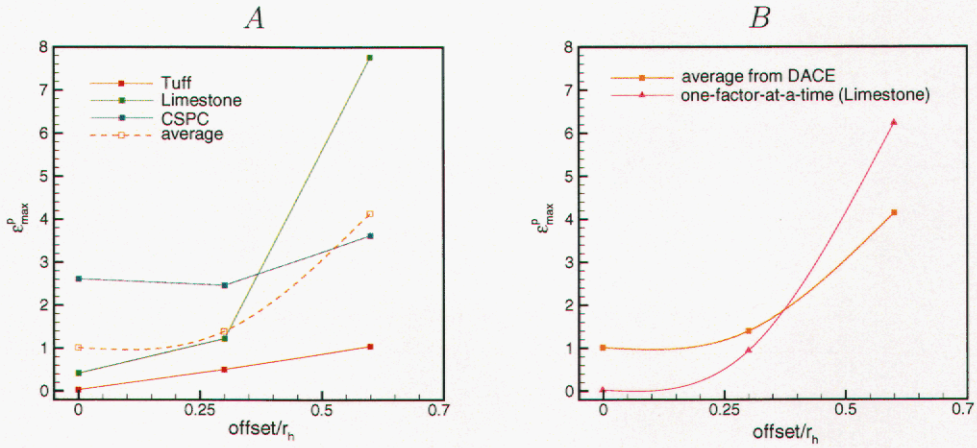

Figure 5.8: Maximum plastic strain as a function of offset.

event. Of course, the specific value of offset/r_h to be tolerated will also depend on the target material, since a decreasing target resistance to penetration will allow for higher penetrator offsets (see simulation results for run 3).

Finally, a mesh refinement study was carried out to determine if the penetrator-target system response is sensitive to the mesh resolution of the target. The target selected for this study has $d_h = 10$ in and $\beta = 0^o$. The conditions of the penetration event are the ones used for Run 2 (see Table 2.3). Three additional meshes were constructed for the target. The meshes are characterized by both a characteristic element dimension "a" along the hole profile and the number of elements used for the target core (see Figure 2.1). The range of values used for "a" is from 0.348 to 0.872 in while the number of finite elements used for the target core ranges from 307989 to 1926746 8-node brick elements. The numerial results are presented in Figure 5.9, which shows the time history of the penetration depth, penetrator deceleration and maximum plastic strain in the penetrator case. It is seen from Figures 5.9–A and 5.9–B that the maximum penetration depth is slightly affected by the target mesh resolution, while the penetrator deceleration is practically unaffected by such refinement. Note that for the penetration depth, the mesh seems to have a greater, although still small, effect on the rebound of the penetrator once the penetrator reaches its maximum depth, with the trend of increased amount of rebound as the mesh is refined. Physically, this rebound is due to the elastic recovery of the target after the penetrator velocity is reduced to zero. Regarding the maximum plastic strain, Figure 5.9–C seems to suggest that the structural response of the penetrator is strongly sensitive to the target mesh. This difference in responses for each mesh starts to be observed before the penetrator reaches its maximum depth, and gets bigger during the penetrator rebound. Further studies are warranted here to get a better insight on this target mesh dependency of the structural response of the penetrator. We note here that these additional studies should include the element death option in PRESTO since this feature may eliminate the observed mesh dependency.

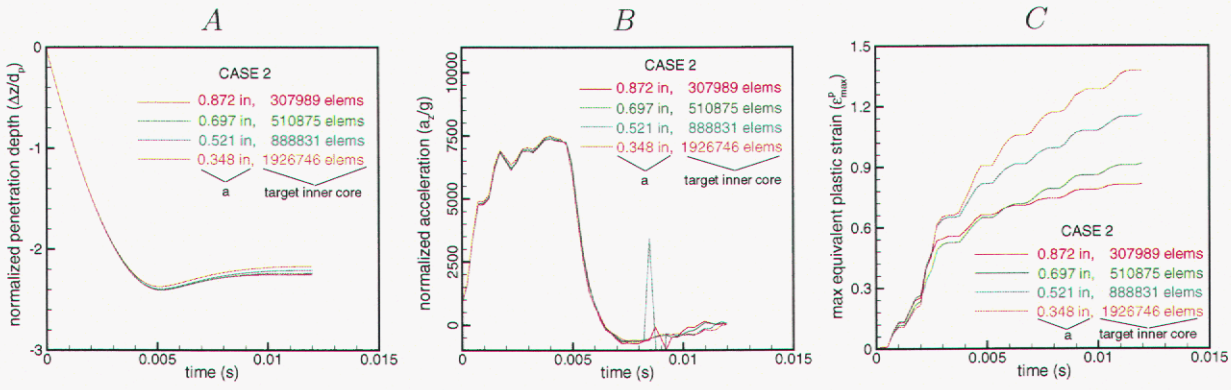

Figure 5.9: Target mesh sensitivity studies. A characteristic dimension of the elements along the hole, indicated by "a", is varied. The number of elements (type hex8) shown corresponds to the mesh of the target inner core.

This page intentionally left blank.

6. SUMMARY

A design and analysis of computer experiments (DACE) approach was used to study pilot-hole assisted penetration events. The study quantified the contribution (main effects) of the chosen seven factors (parameters) to the variability or uncertainty of the selected metrics. The factor's main effects were ranked using main effects plots and one-way ANOVA, with the results:

- Target material and hole diameter are the most influential factors for penetration depth and penetration deceleration, and
- Penetrator offset and target material have the strongest effect on the induced plastic strains of the penetrator case.

The DACE approach was extended to study two factor interaction effects using interaction plots and two-way ANOVA. Interactions are usually present in highly nonlinear problems, such as penetration events. Among the four more important factors affecting each of the metrics, these studies showed that the interaction between offset and target material for the metric ϵ^{p}_{MAX} is the strongest. This result then suggests that penetration studies focusing on the structural analysis of the penetrator case should consider this coupling effect when computing critical loads. Also, a comparison analysis between the DACE and OAT (one-factor-at-a-time) approaches was performed. This analysis shows that the response trends from both studies may be different. This difference is mainly due to the presence of interaction effects that are accounted for in the DACE methodology.

The present study will be used as a starting point for uncertainty quantification analysis of the shaped charge follow through penetrator concept. A specific aspect of this analysis will focus on evaluating/understanding the role of precursor (pilot) holes on reducing target material uncertainties, in particular, when non-uniform or layered targets are involved in the penetration event. In addition, because the numerical simulations carried out in this work indicate that the penetrator nose-case joint is a critical structural part of the penetrator, further design studies are planned to do a detailed structural analysis of this joint. This study will focus on evaluating alternative designs to the one assumed in this work (welded joint). Finally, the target mesh dependency of the structural response of the penetrator

found in this work suggests additional numerical simulations to determine the source of this sensitivity. These simulations should use the element vanishing technique (element death) in PRESTO which could eliminate such mesh dependency.

References

Andersen, J., (2004), Sandia National Laboratories, Livermore, CA, Personal Communication.

Bammann, D.J., (1990), *Modeling the Temperature and Strain Rate Dependent Large Deformation of Metals*, Applied Mechanics Review, **43**, Part 2, 312-319.

Baty, R.S., Lundgren, R.G., and Patterson, W.J., (2003), *On Pilot-Hole Assisted Penetration*, Sandia National Laboratories, NM, SAND2003-0602C.

Campolongo, F., and Saltelli, A., (2000), *Design of Experiments*, in Sensitivity Analysis, Saltelli, A., Chan, K., and Scott, E.M. (Editors), Wiley, New York, p. 51-63.

Chen, E.-P., (1989), *Penetration Into Dry Rocks: A Numerical Study on Friction Simulation*, in Computational Techniques for Contact, Impact, Penetration and Perforation of Solids, Schwer, L.E., Salamon, N.J., and Liu, W.K. (Editors), ASME AMD-Vol. 103, p. 325-336.

Fossum, A.F, and Fredrich, J.T, (2000), *Cap Plasticity Models and Compactive and Dilatant Pre-Failure Deformation*, Pacific Rocks 2000: Rock Around The Rim, A.A. Balkema, 1169-1176

Giunta, A.A., Wojtkiewicz, S.F., and Eldred, M.S., (2003), *Overview of Modern Design of Experiments Methods for Computational Simulations*, AIAA 2003-0649, 41st AIAA Aerospace Sciences Meeting and Exhibiting, January 6-9, Reno, NV.

Hedayat, A.S., Sloane, N.J.A., and Johm Stufken, (1999), *Orthogonal Arrays, Theory and Applications*, Springer-Verlag, New York, p. 20.

MINITAB Statistical Software, Minitab Inc., Release 14.

Patterson, W.J., and Fellerhoff, R.D., (1971), *A Shaped Charge/REB for Enhancing Penetration of Rock and Concrete Targets*, Sandia National Laboratories, NM, SC-DR-71.

Vigil, M.G., (2003), *Design of Largest Shaped Charge: Generation of Very Large Diameter, Deep Holes in Rock and Concrete Structures*, Sandia National Laboratories, NM, SAND2003-1160.

Wu, C.F.J., and Hamada, M., (2000), *Experiments: Planning, Analysis, and Parameter Design Optimization*, Wiley, New York.

DISTRIBUTION

1	MS 0139	P. Yarrington, 9902
1		S.E. Lott, 9902
1	MS 0325	D.J. Frew, 2615
1	MS 0328	J.J. Calderone, 2612
1	MS 0370	T.G. Trucano, 9211
1		S.A. Mitchell, 9211
1		L.P. Swiler, 9211
1	MS 0372	J. Jung, 9127
1	MS 0384	H.S. Morgan, 9140
1	MS 0482	E.R. Hoover, 2131
1		T.C. Togami, 2131
1		J.B. Wirth, 2131
1	MS 0828	M. Pilch, 9133
1	MS 0751	A.L. Fossum, 6117
1		R.M. Brannon, 6117
1	MS 1156	D.S. Preece, 15322
1		V.S. Berg, 15322
1	MS 1160	D.A. Dederman, 15431
1		R.T. Gilchrist, 15431
1		J.E. Lucero, 15431
1	MS 9014	A.R. Ortega, 8242
1		J.R. Andersen, 8241
1	MS 9034	A. McDonald, 8221
1		S.E. Faas, 8221
1		C.D. Scholz, 8221
1	MS 9042	E.P. Chen, 8763
1		D.J. Bammann, 8763

1		D.M. Kwon, 8774
5		M.L. Chiesa, 8774
1		D. Kletzli, 8774
1	MS 9153	D.R. Henson, 8200
1		G.A. Thomas, 8200
1	MS 9154	E.B. Talbot, 8222
1		A.F. Baker, 8222
5		P.M. Booker, 8222
1		A.M. Williams, 8222
1	MS 9159	S.W. Thomas, 8962
1		P.D. Hough, 8962
1		M.L. Martinez-Canales, 8962
1	MS 9161	W.R. Even Jr., 8760
1	MS 9403	J.M. Hruby, 8700
1	MS 9405	K.L. Wilson, 8770
5		E.B. Marin, 8763
1	MS 9409	P.A. Spence, 8754
1		W.G. Houf, 8775
1	MS 0899	Technical Library, 9616
3	MS 9018	Central Technical Files, 8945-1
1	MS 9021	Classification Office, 8511 for Technical Library, MS 0899, 9616 DOE/OSTI via URL